ANNUAL REVIEWS

Annual Review of Nuclear and Particle Science

Something Can Come of Nothing: Surface Approaches to Quantum Fluctuations and the Casimir Force

Giuseppe Bimonte,[1,2] Thorsten Emig,[3] Noah Graham,[4] and Mehran Kardar[5]

[1]Dipartimento di Fisica "Ettore Pancini," Università degli Studi di Napoli Federico II, Complesso Universitario di Monte Sant'Angelo, Napoli, Italy

[2]INFN Sezione di Napoli, Napoli, Italy

[3]Laboratoire de Physique Théorique et Modèles Statistiques, CNRS UMR 8626, Université Paris-Saclay, Orsay, France

[4]Department of Physics, Middlebury College, Middlebury, Vermont, USA; email: ngraham@middlebury.edu

[5]Department of Physics, Massachusetts Institute of Technology, Cambridge, Massachusetts, USA

Annu. Rev. Nucl. Part. Sci. 2022. 72:93–118

First published as a Review in Advance on July 5, 2022

The *Annual Review of Nuclear and Particle Science* is online at nucl.annualreviews.org

https://doi.org/10.1146/annurev-nucl-111119-012402

Keywords

Casimir forces, fluctuation-induced interactions, stress tensor, path integral, scattering matrix

Abstract

The Casimir force provides a striking example of the effects of quantum fluctuations in a mesoscopic system. Because it arises from the objects' electromagnetic response, the necessary calculations in quantum field theory are most naturally expressed in terms of electromagnetic scattering from each object. In this review, we illustrate a variety of such techniques, with a focus on those that can be expressed in terms of surface effects, including both idealized boundary conditions and their physical realization in terms of material properties.

Contents

Nothing can come of nothing.

—*King Lear* (1.1.92)

It's cool, huh? Zero-point energy. I save the best inventions for myself.

—Syndrome, *The Incredibles*

1. INTRODUCTION: THE QUANTUM VACUUM

Since it was first calculated in 1948 (1), the Casimir force between uncharged conducting plates has provided a compelling application of quantum field theory. Proportional to both $\hbar$ and c, it provides a concrete illustration of the effects of relativistic quantum fluctuations in a mesoscopic system. Since then, it has evolved from thought experiment to precision measurement (2–20), and may in the future guide and influence the design and operation of microelectromechanical devices (6, 21).

A standard calculation in undergraduate electromagnetism shows that one can compute the total energy of an electrostatic charge distribution as an integral over space of either the electrostatic interaction energy of all the charges or the energy density in the electric field,

$$U = \frac{1}{2}\int \phi\rho \, d\mathbf{x} = -\frac{\epsilon_0}{2}\int \phi\nabla^2\phi \, d\mathbf{x} = \frac{\epsilon_0}{2}\int \nabla\phi\cdot\nabla\phi \, d\mathbf{x} = \frac{\epsilon_0}{2}\int \boldsymbol{E}^2 \, d\mathbf{x}, \qquad 1.$$

where $\boldsymbol{E}$ is the electric field, ϕ is the electrostatic potential, and ρ is the charge density; the contributions from the surface at infinity are assumed to vanish. Because this derivation requires an integration by parts, it does not imply that the integrands are equal, and only the latter approach yields an energy density consistent with the locality constraints of relativity. From a theoretical point of view, this argument yields the remarkable result that the energy of a parallel plate capacitor is stored not on the plates themselves but rather in the electric field between the plates. However, because any experiments not involving gravitation are sensitive only to the total energy of a system rather than its spatial distribution within that system, in practice both approaches yield equivalent results. Furthermore, by writing the electrostatic potential in terms of Green's function

$G(\mathbf{x}, \mathbf{x}')$, one can express the energy as an interaction between charges:

$$U = \frac{1}{2}\int \phi\rho \, \mathrm{d}\mathbf{x} = \frac{1}{8\pi\epsilon_0}\int\int \rho(\mathbf{x})G(\mathbf{x}, \mathbf{x}')\rho(\mathbf{x}') \, \mathrm{d}\mathbf{x}\mathrm{d}\mathbf{x}' . \quad 2.$$

An exactly analogous situation applies to quantum fluctuations in quantum electrodynamics (QED). As a QED phenomenon, the Casimir energy can be represented in terms of either fluctuating charges and currents or fluctuating fields [and in scattering approaches it is often convenient computationally to pass between the two representations (22)], but it is no more or less a demonstration of the existence of so-called vacuum fluctuations than any other QED process (23). But once one considers gravitational phenomena, these choices become inequivalent, and one must consider the field interpretation to maintain consistency with the equivalence principle (24).

These gravitational effects play a particularly striking role in cosmological dark energy. In any QED calculation, whether it be a mesoscopic Casimir system, an atomic Lamb shift, or a high-energy physics scattering amplitude, one encounters a formally infinite energy corresponding to the zero-point oscillation $\hbar\omega/2$ of all the modes of each quantum field. This infinity can be regularized, so that it is rendered finite by assuming that the quantum field theory is modified at very short distances by new physics that acts as a cutoff on these integrals. However, because that cutoff must be at much shorter distances that those probed by current experiments, the resulting integral would yield an extremely large value, corresponding to an energy density per unit volume of the vacuum. In any measurement of Casimir forces, this large energy cancels and has no observable consequences.

Because the dynamics of the expanding Universe are sensitive to absolute sources of energy rather than simply energy differences, this vacuum energy has major effects in cosmology. These effects are distinctive because a fixed vacuum energy per unit volume has negative pressure: As the Universe expands, the total energy goes up, in contrast to the usual situation in thermodynamics, where an increase in volume corresponds to a decrease in energy. So vacuum energy leads to a relation $\mathrm{d}U = -p\mathrm{d}V$ with negative pressure p, corresponding to a stress–energy tensor that is proportional to the space-time metric. Because this negative pressure appears in three entries of the stress–energy tensor while the positive energy appears only once, the resulting effect on the expansion rate is the opposite of ordinary matter—dark energy accelerates the expansion of the Universe, in contrast to the ordinary forces of gravitational attraction that slow it down. The existence of our observed Universe, however, shows that the actual vacuum energy must be much smaller than one would estimate from the sum over zero-point energies; otherwise, this accelerated expansion would have prevented the formation of stars and galaxies. At first, it was assumed that some unknown mechanism instead canceled their contribution to the gravitational stress–energy tensor. However, "just because it's infinity doesn't mean it's zero": Precision cosmology experiments (25, 26) have offered convincing evidence that there is a nonzero vacuum energy density, just one that is 120 orders of magnitude smaller than what one would expect from an estimate based on the integral over zero-point modes with a short-distance cutoff.

Because Fermi fields obey canonical anticommutation rather than commutation relations, each mode of a Fermi field has zero-point energy $-\hbar\omega/2$ rather than $\hbar\omega/2$. As a result, one might hope that this vacuum energy cancels between Bose and Fermi fields. This proposal is made concrete in theories with supersymmetry, in which every fermionic field has a bosonic partner and vice versa, guaranteeing that the vacuum energy vanishes. However, because supersymmetry is not observed in nature—there is no massless fermionic partner to the photon, for example—supersymmetry must be spontaneously broken, which reintroduces a nonzero vacuum energy density at the associated energy scale. While the resulting vacuum energy density is much smaller than that of the short-distance cutoff, it is still far, far larger than the observed value; because no experimental

evidence for supersymmetry has been observed, the supersymmetry-breaking scale must be well above the scales that have been probed in high-energy physics.

We emphasize that this mystery does not represent a physical or logical inconsistency in the observed energy of the vacuum, however. Like a mass or coupling constant, the vacuum energy is a renormalized parameter in quantum field theory, meaning that it can be fixed to whatever value is dictated by experimental input via the corresponding counterterm in the theory. The bare parameter alone is not physically measurable. In the case of a mass or coupling, however, one can fix the renormalized parameter on the basis of one experiment and then use that value in many other experiments, giving the choice predictive power. For the energy of the vacuum, in effect we have one experiment for one free parameter. As a result, one is motivated to find more sophisticated models in which this parameter can be connected to other properties of the theory that can be fixed independently, using as guidance approaches such as the anthropic principle (27), or nonlinear feedback mechanisms such as quintessence (28) or effective media (29), but how to do so precisely remains an open question.

2. PROXIMITY FORCE APPROXIMATION AND DERIVATIVE EXPANSION

As is typical in classical and quantum field theory, exact analytic calculations are tractable only in problems with a high degree of symmetry. It is therefore invaluable, especially in comparison with experiments, to have convenient approximations available.

Originally developed by Derjaguin (30) in the context of surface adhesion and colloids, the proximity force approximation (PFA) relates forces between gently curved objects at close separations, $\sim d$, to the corresponding interactions between flat surfaces over an area set by the local radii of curvature, $\sim R$. In this approach, one approximates the Casimir energy between two surfaces as the local interaction between flat parallel plates:

$$E_{\mathrm{PFA}} = \int_{\Sigma} \mathrm{d}\mathbf{x}\, U(z), \qquad 3.$$

where z is the local distance between the surfaces and $U(z)$ is the energy per unit area for parallel plates made of the same materials, which is given below in Equation 9 for the case of ideal boundaries. Here the integral is over the surface Σ, which can be taken as one of the two interacting surfaces or as a reference surface placed between them. Because this approximation ignores the effects of nonparallelism of the interacting surfaces, it can depend on the choice of Σ, meaning that a different choice may lead to a better or worse approximation.

PFA is widely used to estimate Casimir (1) and van der Waals (31) forces, starting with the Lifshitz formula (32) for the interaction between parallel plates, and it is asymptotically exact as $d/R \to 0$. However, the range of validity of this approximation, and the nature of subsequent correction terms to PFA, was previously unknown. A conceptual breakthrough in 2011 (33) showed that earlier perturbative corrections to parallel plate forces (34, 35) can be organized into a gradient expansion in the local separation between surfaces for the force between gently curved bodies, implementing this program for scalar fields. Recognizing the usefulness of this approach, Reference 36 generalized the gradient expansion of Reference 33 to practical computations of the electromagnetic (EM) Casimir force and tested the validity of the PFA corrections against exact results for the force between a perfectly conducting sphere and plate. The extension to real materials described by a (frequency-dependent) dielectric response $\epsilon(\omega)$ is not trivial and was developed in Reference 37. In particular, this study obtained an explicit expression for the PFA correction to the force gradient using the dielectric function of gold, at room temperature. The corrections to the Casimir free energy were found to scale logarithmically with distance, with an unexpectedly

large temperature dependence. Further research (38) considered the effects of roughness or surface modulations. The gradient expansion has now been confirmed against a number of exact results for spheres and cylinders (39), as well as in experiments with corrugated surfaces (40).

2.1. The Gradient Expansion from Resummation of Perturbation Theory

Consider two bodies with gently curved surfaces described by (single-valued) height profiles $z = H_1(\mathbf{x})$ and $z = H_2(\mathbf{x})$, with respect to a reference plane Σ, where $\mathbf{x} \equiv (x, y)$ are Cartesian coordinates on Σ and the z axis is normal to Σ. The intervening quantum field can be a scalar or EM field. For the scalar case, we can impose either Dirichlet or Neumann boundary conditions. The EM case, for ideal (mirror) boundaries, is obtained simply as the sum of Dirichlet and Neumann cases, corresponding to the two transverse polarizations. Extension to the case of real materials, described by a complex dielectric permittivity, is possible. The only restriction on the boundary conditions is that they should describe homogeneous and isotropic materials, so that the Casimir energy is invariant under simultaneous translations and rotations of the two profiles in the plane Σ.

The gradient expansion postulates that the Casimir energy, when generalized to two surfaces and to arbitrary fields subject to arbitrary boundary conditions, is a functional $E[H_1, H_2]$ of the heights H_1 and H_2, which has a derivative expansion

$$\begin{aligned} E[H_1, H_2] = \int_\Sigma \mathrm{d}\mathbf{x}\, U(H)\, [1 &+ \beta_1(H)\nabla H_1 \cdot \nabla H_1 \\ &+ \beta_2(H)\nabla H_2 \cdot \nabla H_2 + \beta_\times(H)\nabla H_1 \cdot \nabla H_2 \\ &+ \beta_-(H)\,\hat{\mathbf{z}} \cdot (\nabla H_1 \times \nabla H_2) + \ldots], \end{aligned} \qquad 4.$$

where $H(\mathbf{x}) \equiv H_2(\mathbf{x}) - H_1(\mathbf{x})$ is the height difference and the dots denote higher derivative terms. Here, $U(H)$ is the energy per unit area between parallel plates at separation H; translation and rotation symmetries in $\mathbf{x}$ permit only four distinct gradient coefficients at lowest order, $\beta_1(H)$, $\beta_2(H)$, $\beta_\times(H)$, and $\beta_-(H)$. The form of such a local expansion is motivated by the existence of well-established derivative expansions of scattering amplitudes (41) from which the Casimir energy can be derived (22). Arbitrariness in the choice of Σ constrains the coefficients β in the above expansion. Invariance of E under a parallel displacement of Σ requires that all the βs depend only on the height difference H and not on the individual heights H_1 and H_2. These coefficients are further constrained by the invariance of E with respect to tilting the reference plate Σ. Under a tilt of Σ by an infinitesimal angle ϵ in the (x, z) plane, the height profiles H_i undergo a change by $\Delta H_i = -\epsilon[x + H_i(\partial H_i/\partial x)]$, and the requirement that E not change implies

$$\begin{aligned} 2[\beta_1(H) + \beta_2(H)] + 2\,\beta_\times(H) + H\,\frac{\mathrm{d}\log U}{\mathrm{d}H} - 1 = 0, \\ \beta_-(H) = 0, \end{aligned} \qquad 5.$$

so that the nonvanishing cross term $\beta_\times$ is determined by β_1, β_2, and U.

Equation 5 indicates that, to second order in the gradient expansion, the two-surface problem reduces to that of a single curved surface facing a plane. Therefore, U, β_1, and β_2 can be determined by setting H_1 or H_2 to zero. Let us set H_1 to zero and define $\beta_2(H) \equiv \beta(H)$. We can then determine the exact functional dependence of $\beta(H)$ on H by comparing the gradient expansion in Equation 4 to a perturbative expansion of the Casimir energy around flat plates, to second order

in the deformation. For this purpose, we take Σ to be a planar surface and decompose the height of the curved surface as $H(\mathbf{x}) = d + h(\mathbf{x})$, where d is chosen to be the distance of closest separation. For small deformations $|h(\mathbf{x})|/d \ll 1$, we can expand $E[0, d + h]$ as

$$E[0, d + h] = A\,U(d) + \mu(d)\tilde{h}(\mathbf{0}) + \int \frac{d\mathbf{k}}{(2\pi)^2} G(k; d)|\tilde{h}(\mathbf{k})|^2, \qquad 6.$$

where A is the area, $\mathbf{k}$ is the in-plane wave vector, and $\tilde{h}(\mathbf{k})$ is the Fourier transform of $h(\mathbf{x})$. The kernel $G(k; d)$ has been evaluated by several authors: in Reference 34 for a scalar field fulfilling Dirichlet or Neumann boundary conditions on both plates, as well for the EM field satisfying ideal metal boundary conditions on both plates, and in Reference 35 for the EM field with dielectric boundary conditions. For a deformation with small slope, the Fourier transform $\tilde{h}(\mathbf{k})$ is peaked around zero. Because the kernel can be expanded at least through order k^2 about $k = 0$ (41), we define

$$G(k; d) = \gamma(d) + \delta(d)\,k^2 + \ldots. \qquad 7.$$

For small h, the coefficients in the derivative expansion can be matched with the perturbative result. By expanding Equation 4 in powers of $h(\mathbf{x})$ and comparing the result with the perturbative expansion to second order in both $\tilde{h}(\mathbf{k})$ and k^2, we obtain

$$U'(d) = \mu(d), \quad U''(d) = 2\gamma(d), \quad \beta(d) = \frac{\delta(d)}{U(d)}, \qquad 8.$$

where the prime symbol denotes a derivative.

2.2. Ideal Boundaries

For ideal boundary conditions (Dirichlet or Neumann for a scalar field, or perfect mirrors for the EM field) the energy per unit area between parallel plates with separation d is given by

$$U(d) = -\alpha \frac{\pi^2 \hbar c}{1,440 d^3}. \qquad 9.$$

The overall coefficient is $\alpha = 1$ for scalar field fluctuations where both surfaces have either Dirichlet or Neumann boundary conditions, $\alpha = 2$ (corresponding to the two polarizations) for EM fluctuations with perfect conductor boundary conditions, and $\alpha = -7/8$ for a scalar field with mixed Neumann/Dirichlet boundaries.

By using Equation 8 and the appropriate perturbation series, one can compute the coefficient β for the following five cases: a scalar field obeying Dirichlet or Neumann boundary conditions on both surfaces; Dirichlet boundary conditions on the curved surface and Neumann boundary conditions on the flat, or vice versa; and the EM field with ideal metal boundary conditions. Because in all these cases the problem involves no other length apart from the separation d, β is a pure number. β_{D} was first computed in Reference 33, which found $\beta_{\mathrm{D}} = 2/3$. Reference 36 then found $\beta_{\mathrm{N}} = 2/3\,(1 - 30/\pi^2)$, $\beta_{\mathrm{DN}} = 2/3$, $\beta_{\mathrm{ND}} = 2/3 - 80/7\pi^2$ (where the subscripts DN and ND denote the curved-surface and flat-surface boundary conditions, respectively), and $\beta_{\mathrm{EM}} = 2/3\,(1 - 15/\pi^2)$. Upon solving Equation 5, one finds $\beta_\times = 2 - \beta_1 - \beta_2$, where both β_1 and β_2 are chosen to be equal to either β_{D} and β_{N} or β_{EM}, for the case of identical boundary conditions on the two surfaces, or rather $\beta_1 = \beta_{\mathrm{DN}}$ and $\beta_2 = \beta_{\mathrm{ND}}$ for the case of a scalar field obeying mixed ND boundary conditions.

Using the above values for β and $\beta_\times$, one can evaluate the leading correction to PFA by explicitly evaluating Equation 4 for the desired profiles. For example, for two spheres of radii R_1 and R_2,

both with the same boundary conditions for simplicity, we obtain

$$E = E_{\mathrm{PFA}}\left[1 - \frac{d}{R_1 + R_2} + (2\beta - 1)\left(\frac{d}{R_1} + \frac{d}{R_2}\right)\right], \qquad 10.$$

where $E_{\mathrm{PFA}} = -(\alpha\pi^3\hbar c R_1 R_2)/[1, 440d^2(R_1 + R_2)]$. The corresponding formula for the sphere–plane case can be obtained by taking one of the two radii to infinity. These results are in good agreement with analytic calculations in the sphere–plane system (39, 42).

2.3. Material Boundaries

The approach described above, which converts a perturbative expansion in small deformations to a gradient expansion, can be performed for any cases where a perturbative expansion is possible. These include the case of two infinitely thick plates separated by d, each modeled as a homogeneous and isotropic dielectric material, with frequency-dependent permittivities $\epsilon_1(\omega)$ and $\epsilon_2(\omega)$. Much like the crossover between retarded and nonretarded van der Waals interactions, the Casimir force also becomes dependent on material properties through $\epsilon(\omega)$ at short distances (typically in the range of 10–100 nm). If the dielectric response is dominated by a resonance at a single characteristic frequency $\overline{\omega}$, in the so-called near-field regime of separations $d \leq c/\overline{\omega}$, then the Casimir energy density in Equation 9 changes from $U(d) \propto \hbar c/d^3$ to $U(d) \propto \hbar\overline{\omega}/d^2$.

Because $U(d)$ still diverges as $d \to 0$ even in the near-field regime, PFA and the gradient expansion should still be applicable. This calculation was implemented in Reference 37, which applied this method to two infinitely thick plates composed of homogeneous and isotropic dielectric materials, with general permittivities $\epsilon_1(\omega)$ and $\epsilon_2(\omega)$. The resulting corrections to PFA are no longer pure numbers but rather depend on temperature and separation (through material-dependent parameters). While we do not reproduce the details here, we note that they have in fact been used for comparison to sphere–plate experiments (40, 43, 44).

In principle, we may anticipate a gradient expansion for any situation when a shape-dependent quantity diverges sufficiently rapidly as a function of separation. One example, described in Reference 38, involves radiative heat transfer (RHT) between objects at different temperatures. The heat transfer between parallel plates at large distances is dominated by propagating photons and is independent of separation d. However, as noted by Polder & Van Hove (45), RHT at short separation increases strongly upon decreasing separation because of tunneling of evanescent EM waves across the vacuum gap. The precise form of this enhancement depends on the material properties: If the response of the material can be characterized by a single dominant frequency $\overline{\omega}$, then in the near-field regime of $d \leq c/\overline{\omega}$, RHT diverges as $S(d) \propto \hbar\overline{\omega}^2/d^2$ (46). RHT due to evanescent waves has also attracted a lot of interest because of its connection with scanning tunneling microscopy and scanning thermal microscopy under ultrahigh-vacuum conditions (47, 48). The enhancement of heat transfer in the near-field regime (generally denoting separations that are small in comparison to the thermal wavelength, which is roughly 8 μm at room temperature) has only recently been verified experimentally (49, 50).

Much like PFA, the leading term for RHT between closely spaced curved objects has been computed by use of a corresponding proximity transfer approximation (PTA) (51–53). Reference 46 extended a gradient expansion approach to compute the first correction to PTA, which can be expressed as a spectral decomposition, with a correction factor $\beta(\omega)$ at each frequency.

2.4. Further Applications

While the above examples focus on two surfaces, the gradient expansion can also be applied to estimate the interaction between a polarizable particle and a gently curved surface. For a particle of

polarizability α, the Casimir–Polder force (54) due to a flat surface scales with the separation d as $\alpha \times \hbar c/d^4$ in the far field and as $\alpha \times \hbar\overline{\omega}/d^3$ in the near field. Perturbative results for the interaction of the particle with a slightly modulated surface can again be converted to a gradient expansion for the force close to a curved surface. Reference 55 showed that the leading correction on approaching a surface with profile $H(\mathbf{x})$ depends on its curvature, proportional to $d\nabla^2 H$, while the next order scales as $(d\nabla^2 H)^2$. If the polarizable particle is a molecule, Reference 56 demonstrates that, in principle, the shift of its rotational levels due to Casimir–Polder interactions can be used as a probe of the surface profile.

3. THE SCATTERING APPROACH AND ITS APPLICATIONS

The calculations we have studied in the previous section are based on local approximations. Scattering methods provide a complementary approach, based on the global EM response of each object in a Fourier scattering basis. As a result, this approach provides exact expressions that are applicable to both concrete calculations and broader theoretical analyses.

The fundamental idea of the scattering approach is to decompose the combined quantum fluctuations of a pair of objects in terms of the fluctuations of each object individually, combined with a propagator that carries these fluctuations from one object to another. The result is the so-called TGTG form combining the scattering T matrix (57, 58) for each object with the free Green's function propagator (59). The material and geometric properties of each object are represented through its individual T matrix, independently of the other objects, while the propagator captures information about the objects' relative position and orientation but is independent of the properties of the objects themselves. Because the scattering matrices for different objects are often most naturally written in different bases—for example, spherical and Cartesian coordinates for a sphere–plane system—the relevant change of basis may also be needed in combining these expressions. Finally, the sum over all possible fluctuations is introduced as a log determinant or, equivalently, a trace log, which in practice is expressed as an integral over frequencies and a sum over scattering channels, with the former typically Wick rotated to the imaginary frequency axis.

Scattering theory methods were first applied to the parallel plate geometry by reformulating Lifshitz theory in terms of reflection coefficients (60). These efforts led to a derivation of the Lifshitz formula using reflection coefficients for lossless infinite plates (61) and its extensions to lossy case (62) and nonspecular (63) reflection. Around the same time, the multiple-scattering approach to the Casimir energy for perfect metal objects was developed, making it possible to compute the Casimir energy at asymptotically large separations (64, 65) at both zero and nonzero temperatures. In this approach, information about the conductors is encoded in a local surface scattering kernel.

Another scattering-based approach has been to express the Casimir energy as an integral over the density of states of the fluctuating field, using the Krein formula (66–68) to relate the density of states $\rho(k)$ to the $\mathcal{S}$ matrix for scattering from the ensemble of objects:

$$\rho(k) = \frac{1}{2\pi i} \operatorname{Tr} \frac{\mathrm{d}}{\mathrm{d}k} \log \mathcal{S}(k). \qquad 11.$$

This $\mathcal{S}$ matrix is difficult to compute in general, but the use of many-body scattering of scalar fields made it possible to connect the $\mathcal{S}$ matrix of a collection of spheres (69) or disks (70) to the objects' individual $\mathcal{S}$ matrices, which are easy to find. Subsequent research combined this result with the Krein formula to investigate the scalar and fermionic Casimir effect for disks and spheres (71–73). Casimir energies of solitons in renormalizable quantum field theories have been computed using scattering theory techniques that combine analytic and numerical methods (74).

References 75 and 76 introduced path integral methods to the study of Casimir effects and used them to investigate the EM Casimir effect for two parallel perfect metal plates. Similar methods were used to study the scalar thermal Casimir effect for Dirichlet, Neumann, and mixed boundary conditions in References 77 and 78. This approach was adapted to the quantum case and developed further in References 79 and 80. It was subsequently applied to the quantum EM Casimir interaction between plates with roughness (34) and between deformed plates (81). Finally, the path integral approach was connected to scattering theory in Reference 82.

Because this approach relies on the fundamental formalism of quantum field theory, it has a wide range of applications to problems involving quantum (and, as discussed below, thermal) fluctuations. To our knowledge, it was first developed in precise detail for Casimir calculations in Reference 83. A typical result in this approach takes the form (59, 84, 85)

$$\mathcal{E} = \frac{\hbar c}{2\pi} \int_0^\infty d\kappa \log\det(1 - G_{21}T_1G_{12}T_2), \qquad 12.$$

where T_i are the scattering T matrices (57, 58) for each object and G_{12} and G_{21} are the free Green's functions, which propagate fluctuations in the scattering basis of one object to the scattering basis of the other. Here we have considered only two objects, but this approach has a natural extension to larger numbers of objects (22, 86–88).

By making use of the identity

$$\log\det(1 - A) = \mathrm{Tr}\,\log(1 - A) = -\,\mathrm{Tr}\sum_{j=0}^{\infty}\frac{A^j}{j} \qquad 13.$$

for $A = G_{21}T_1G_{12}T_2$, we can build an intuitive picture of the physics that this formula captures. The T matrix T_1 describes a quantum fluctuation on object 1. The Green's function G_{12} then propagates this fluctuation from object 1 to object 2, the T matrix T_2 describes the fluctuation that results from its interaction with object 2, and finally the Green's function G_{21} propagates this result back to object 1. The sum captures all possible numbers of round-trip reflections, while the trace sums over all possible fluctuation modes with a particular frequency and the integral sums over all frequencies, here having been Wick rotated to imaginary wave number $i\kappa = k = \omega/c$.

To demonstrate the practical application of the formula in Equation 12, we consider the simple case of two isotropic particles (such as atoms or nanoparticles), which are small in comparison to their separation d. We assume that the particles have only electric dipole polarizabilities α_1 and α_2, respectively, which are independent of frequency. (The latter is justified in the retarded limit, where d is much larger than the speed of light divided by a characteristic frequency below which α_j become static.) Then the Green's functions and the T matrices in Equation 12 can be expressed in terms of spherical dipole waves, yielding (3×3)-dimensional matrices. The T matrices are diagonal, given by

$$T_{j;mm'} = \frac{2}{3}\alpha_j\kappa^3\delta_{mm'} \qquad 14.$$

for $j = 1$ or 2 and $m = -1$, 0, or 1. With the dipole expansion of the Green's functions G_{12} and G_{21}, one obtains, after taking the determinant in Equation 12, the energy

$$\mathcal{E} = -\frac{\hbar c}{\pi d}\frac{\alpha_1}{d^3}\frac{\alpha_2}{d^3}\int_0^\infty du(3 + 6u + 5u^2 + 2u^3 + u^4)e^{-2u}, \qquad 15.$$

where we have set $u = \kappa d$ and expanded the logarithm around one because $\alpha_j \ll d^3$. Integration easily yields

$$\mathcal{E} = -\frac{23}{4\pi}\hbar c\frac{\alpha_1\alpha_2}{d^7}, \qquad 16.$$

which is the so-called Casimir–Polder potential.

As an exact expression, Equation 12 can be used to prove general results applicable to arbitrary geometries. For example, Reference 59 applies a Feynman–Hellmann argument to show that the force between any configuration of EM conductors with mirror symmetry is always attractive, a result that informs our discussion below of Casimir stresses on an individual object. It can also be used to demonstrate a form of Earnshaw's theorem, ruling out the existence of a stable equilibrium generated by Casimir forces (89).

For experimental research, spherical, cylindrical, and planar geometries are by far the most common and useful. As first detailed in Reference 83, one can use a multipole basis to express scattering from each object in its own partial-wave basis, and then use expansions of the free Green's function to translate scattering from one object's basis to another (22, 85, 87, 90). This approach has been adapted to a wide range of calculations for plane (63), cylinder, cylinder–plane, and cylinder–sphere geometries (22, 84, 91, 92); sphere geometries for both scalar (72, 73, 87) and EM (22, 85) fluctuations; and, most importantly for experiments, sphere–plane geometries in electromagnetism (86, 93, 94).

3.1. Geometries with Edges and Tips

Scattering methods are much more tractable for objects with geometries for which the T matrix is diagonal. One can extend the range of such situations by considering more unusual coordinate systems. For scalar fluctuations, these include elliptic cylinder (95), parabolic cylinder (96), and spheroidal geometries (97), for which limiting cases are a finite-width strip, a half-plane, and a disk, respectively. One can also consider scattering in a different variable in order to study a wedge or cone using ordinary cylindrical and spherical coordinates, respectively (98). In these cases, one uses contour integration to replace the scattering theory sum over partial waves with a continuous integral. One can also consider complementary geometries by using systems with planar gaps (99) and by applying the generalization of Babinet's principle (100), and for scalar theories one can apply worldline methods (101).

For perfect conductors, all of these cases can be extended to electromagnetism except for spheroidal scattering, as any translation-invariant geometry can be decomposed into polarizations obeying Dirichlet and Neumann boundary conditions, and scattering from a cone can also be diagonalized through analytic continuation of the standard techniques of Mie scattering. The limiting case of the perfectly conducting disk can nonetheless be solved exactly as an analytic calculation in oblate spheroidal coordinates (102, 103), for which the scattering matrix is no longer diagonal.

The wedge, parabolic cylinder, and elliptic cylinder results can be combined to yield a consistent model of the effects of edges (104–106). The result can be expressed as an approximate form of the Casimir energy per unit length of a perfectly conducting strip parallel to a perfectly conducting plane:

$$\frac{\mathcal{E}}{\hbar c L} = -\frac{\pi^2}{720}\frac{2d}{H^3} + \frac{2\beta}{H^2} + \frac{\gamma}{2dH} + \dots. \qquad 17.$$

Here H is the separation between the strip and the plane, $2d$ is the width of the strip, and $\beta = 0.00092$ and $\gamma = -0.0040$ are numerical parameters capturing the effect of a single edge and the interaction between two edges, respectively; the result for β is consistent with limiting cases of the wedge and parabolic cylinder. One can also obtain the energy per unit length of a perfectly conducting half-plane perpendicular to a perfectly conducting plane as (96)

$$\frac{\mathcal{E}}{\hbar c L} = \int_0^\infty \frac{q\,dq}{4\pi} \log\det[\mathbb{1}_{\nu\nu'} - (-1)^\nu \mathrm{k}_{-\nu-\nu'-1}(2qH)] = -\frac{C_\perp}{H^2}, \qquad 18.$$

where H is the separation distance, $\mathrm{k}_\ell(u)$ is the Bateman k-function (107), the determinant is over $\nu, \nu' = 0, 1, 2, 3\ldots$, and $C_\perp = 0.0067415$ is obtained by numerical integration.

3.2. Casimir Stresses

An interesting extension of Casimir force calculations is to the case of Casimir stresses on a single object. This problem is harder to define than the case of forces between rigid bodies, because deformation of a single object requires a variation of the physical configuration of an object, rather than simply a variation of the position of fixed objects. As a result, the formally infinite contributions localized on the object no longer cancel, and we must apply renormalization techniques. These in turn require a model of the object's material properties.

Debates about Casimir stresses originate from an early model of the electron as a charged shell for which attractive Casimir forces balance Coulomb repulsion (108). Here the dynamics of the shell are assumed as a definition of the fundamental interactions. One finds that specifying an ideal conductor boundary condition leads to a positive energy, and hence expansion of the shell (109–111), invalidating the model's original premise. Of course, modern QED provides a well-verified description of the electron within the broader framework of renormalized quantum field theory.

This result has often been misinterpreted, however, to imply that a conducting shell will experience a repulsive stress. This case is very different, because the dynamics of an actual piece of conducting material are determined by the underlying physics of the matter that makes it up and so cannot be assumed to implement an ideal boundary condition at all frequencies. [The Casimir energy of an idealized boundary can be of interest for the mathematical Weyl problem of the relationship between eigenvalue spectra and geometry (112, 113).] A repulsive stress is also in conflict with the well-established attractive Casimir force between conductors; in particular, the force between two hemispheres, as in any configuration of conductors with mirror symmetry, is always attractive (59). Similarly, while a boundary condition calculation yields a repulsive stress on a rectangular solid, the force on a piston is attractive, as has been shown in two dimensions (114) and three dimensions (115), where the latter was derived using a geometrical optics approximation (116).

The resolution of this puzzle lies in contributions from within the material, which no longer cancel when the body is not rigid. Modeling the material as a position-dependent dielectric (117) shows that the contribution from within the material is attractive as well as larger in magnitude than the repulsive external contribution. In the limit where the dielectric becomes infinitely strong, the sphere becomes a conductor (118), but this limit does not commute with the limits involved in renormalization: The theory must be cut off at a high enough frequency that the material is transparent. Qualitatively similar results have been obtained by considering specific materials rather than a generic dielectric, such as a carbon nanostructure (119) or a so-called fish-eye medium (120). These findings are also in agreement with research by Deutsch and Candelas (121, 122), who showed that divergences in Casimir stresses arise from surface counterterms (123) that cannot be removed by renormalization, as well as with more detailed calculations in models with a fluctuating scalar field (124–126).

A key aspect of this research is that divergences associated with an ideal boundary arise in two different ways: the "sharp" limit of infinitesimal thickness and the "strong" limit of strong potential. For stresses on a real material, these limits are intertwined. For example, as a spherical shell expands and increases its surface area, it becomes thinner, leading to a weaker EM response. A precise description of this situation requires detailed information about the material's EM properties, but one can gain a qualitative understanding by approximating this behavior via renormalization counterterms. In this process, one introduces a short-distance cutoff, which in a material represents a length scale set by the lattice spacing. The formally divergent contributions

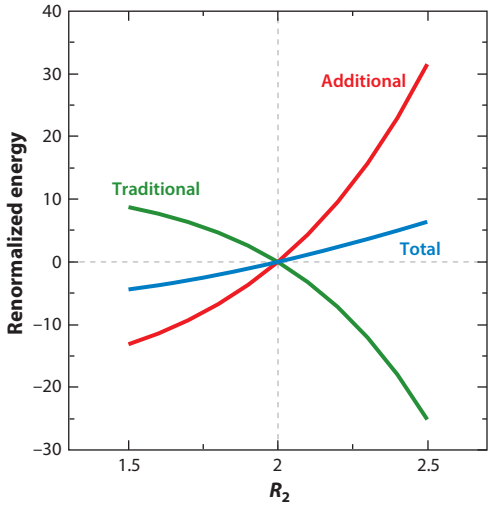

Figure 1

Difference in renormalized energy between shells of radii R_2 and R_1, as a function of R_2 in units where $R_1 = 2$, for generic values of the Drude plasma wavelength and conductivity. The attractive effect of the additional contribution from fluctuations within the material reverses the repulsive traditional contribution from fluctuations outside the material. Figure adapted from Reference 117 (CC BY 4.0).

that arise for a conducting material at short wavelength are then combined with cutoff-dependent counterterms, which are fixed so that the combined result matches experimental inputs. For a stress calculation, one must then fix the dependence of these inputs on the geometry. A reasonable estimate is to assume that the overall strength of the potential, integrated over volume, remains constant, roughly corresponding to holding the total number of charge carriers constant. In scalar models (124–126) one can also adjust the strength of the potential used to model the object's scattering response, while for EM models it is more appropriate to use a Drude model dielectric with fixed plasma wavelength and conductivity and instead vary the thickness of the material so that its volume remains constant.

While this result does not precisely model a particular material like the examples listed above, it allows for a generic description of the discrepancy between the apparent repulsive stress on a spherical conducting shell with the generally attractive Casimir force for dielectric materials, including their perfectly conducting limit. What one finds (117) is that the Casimir self-energy decomposes into a sum of two terms: the traditional contribution due to the shell's external EM response and an additional contribution localized within the thickness of the shell, which consists of a renormalized integral over r. The former reproduces the Boyer result in the conducting limit, but the latter is of comparable magnitude with opposite sign and renders the full result attractive (**Figure 1**).

4. UNIFIED BULK AND SURFACE FORMULATION

While the scattering theory method offers an elegant way of expressing Casimir interaction energies that can be used both to obtain analytic results and to carry out precise calculations in semianalytic form, it also suffers from significant limitations. For objects without a high degree of symmetry, the T matrix is off-diagonal and therefore more difficult to calculate. At the same time, as the separation between the objects decreases, higher frequencies and partial waves become

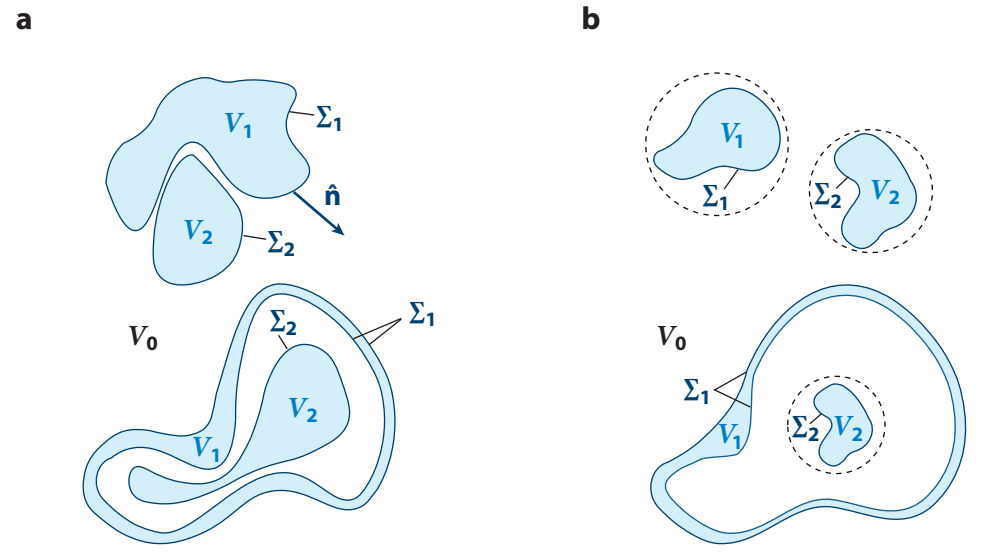

Figure 2

Configuration of dielectric bodies. (*a*) General shapes and positions that can be studied either by integrating the Maxwell stress tensor over a closed surface enclosing the body, directly yielding the Casimir force, or by integrating over all electromagnetic gauge field fluctuations in a path integral, yielding the Casimir free energy. (*b*) Nonpenetrating configurations that can be studied within the scattering approach. Figure adapted from Reference 130 (CC BY 4.0).

important as the calculation becomes dominated by contributions from waves near the point of closest approach (127), so the numerical cutoffs in both the trace over modes and the integral over wave number must be extended to larger and larger values, putting more stress on the numerical algorithms. Taking this case to an extreme, one can imagine a situation where objects interpenetrate within the relevant scattering basis—for example, if scattering from object 1 is computed in a spherical basis and object 2 does not sit entirely outside a sphere enclosing object 1 (**Figure 2*a***), then the expansion fails entirely. From an experimental point of view, however, these kinds of short-distance configurations can be the most appealing, as they represent situations where the force is strongest.

Surface methods (128) can provide an alternative approach that overcomes these limitations. The surface approach was introduced in the literature as a method for a purely numerical computation of Casimir interactions (129). Two different methods to implement the computation of Casimir forces from fluctuating currents exist: One can either integrate the Maxwell stress tensor over a closed surface enclosing the body, directly yielding the Casimir force, or integrate over all EM gauge field fluctuations in a path integral, yielding the Casimir free energy. We review both approaches here.

In comparison to scattering theory–based approaches, the surface formulation has the advantage of not requiring the use of eigenfunctions of the vector wave equation, which are specific to the shapes of the bodies. As a result, this approach is applicable to general geometries and shapes, including interpenetrating structures. The power of the surface approach has been demonstrated by numerical implementations in Reference 129, where it was used to compute the Casimir force in complicated geometries.

Recent research has demonstrated the equivalence of a surface current approach and bulk scattering methods (130). This result can be considered the Casimir analog of the Huygens

equivalence principle (131), which shows that the EM effects of an arbitrary current distribution contained within a closed surface can be exactly reproduced by an equivalent current distribution located on the surface. The main recent advances are (*a*) a new, compact, and elegant derivation of the Casimir force from the Maxwell stress tensor within both a T operator approach and a surface operator approach; (*b*) a new surface formula for the Casimir free energy expressed in terms of a surface operator; and (*c*) a new path integral–based derivation of a Lagrangian and Hamiltonian formulation for the Casimir free energy. Below, we review the main concepts and results of the stress tensor and path integral formulations of the surface current–based approach.

Figure 2*a* shows the geometries and shapes to which the approaches can be applied. For comparison, **Figure 2*b*** displays the nonpenetrating bodies to which scattering theory–based approaches are limited. In general, we assume a configuration composed of N bodies with dielectric functions $\epsilon_r(\omega)$ and magnetic permeabilities $\mu_r(\omega)$, where $r = 1, \ldots, N$. The bodies occupy the volumes V_r with surfaces Σ_r and outward-pointing surface-normal vectors $\hat{\mathbf{n}}_r$. The space with volume V_0 in between the bodies is filled by matter with dielectric function $\epsilon_0(\omega)$ and magnetic permeability $\mu_0(\omega)$.

4.1. Stress Tensor Approach

The common starting point of both the bulk and surface approaches to computing Casimir forces between two or more bodies is the physical picture that the vacuum surrounding the bodies is filled with quantum and thermal fluctuations of the EM field. If the bodies are in thermal equilibrium with the environment at temperature T, then the correlators of the EM field can be derived from linear response theory (132):

$$\begin{aligned}
\langle \hat{E}_i(\mathbf{x},t)\hat{E}_j(\mathbf{x}',t')\rangle_{\mathrm{sym}} &= \hbar\int_{-\infty}^{\infty}\frac{d\omega}{2\pi}\coth\left(\frac{\hbar\omega}{2k_{\mathrm{B}}T}\right)\mathrm{Im}[\mathcal{G}_{ij}^{(EE)}(\mathbf{x},\mathbf{x}',\omega)]\; e^{-i\omega(t-t')},\\
\langle \hat{H}_i(\mathbf{x},t)\hat{H}_j(\mathbf{x}',t')\rangle_{\mathrm{sym}} &= \hbar\int_{-\infty}^{\infty}\frac{d\omega}{2\pi}\coth\left(\frac{\hbar\omega}{2k_{\mathrm{B}}T}\right)\mathrm{Im}[\mathcal{G}_{ij}^{(HH)}(\mathbf{x},\mathbf{x}',\omega)]\; e^{-i\omega(t-t')},\\
\langle \hat{E}_i(\mathbf{x},t)\hat{H}_j(\mathbf{x}',t')\rangle_{\mathrm{sym}} &= \hbar\int_{-\infty}^{\infty}\frac{d\omega}{2\pi}\coth\left(\frac{\hbar\omega}{2k_{\mathrm{B}}T}\right)\left\{-\mathrm{i}\,\mathrm{Re}[\mathcal{G}_{ij}^{(EH)}(\mathbf{x},\mathbf{x}',\omega)]\right\} e^{-i\omega(t-t')}, \qquad 19.
\end{aligned}$$

where the subscript sym on the average symbols denotes the symmetrized products of field operators, and $\mathcal{G}_{ij}^{(\alpha\beta)}(\mathbf{r},\mathbf{r}',\omega)$ (with $\alpha, \beta = E, H$) are the Fourier transforms of the classical Green's functions for the system of bodies. The latter Green's functions are obtained by solving the macroscopic Maxwell equations, subjected to the appropriate boundary conditions on the surfaces of the bodies. We emphasize that Equation 19 includes both zero-point (i.e., quantum) and thermal fluctuation of the EM field. The validity of Equation 19 is subject to the condition that the length scales of the relevant fluctuations should be large compared with atomic distances, such that the EM material properties of the bodies can be described by their macroscopic response functions. For simplicity, we assume that the bodies are made out of homogeneous and isotropic magnetodielectric materials, characterized by the respective frequency-dependent electric and magnetic permittivities $\epsilon(\omega)$ and $\mu(\omega)$.

The mechanical effects of the fluctuating EM field on the bodies are determined by the expectation value $\langle T_{ij}\rangle$ of the Maxwell stress tensor,

$$\langle T_{ij}(\mathbf{x})\rangle = \frac{1}{4\pi}\left\{\langle E_i(\mathbf{x})E_j(\mathbf{x})\rangle + \langle H_i(\mathbf{x})H_j(\mathbf{x})\rangle - \frac{1}{2}\delta_{ij}\left[\langle E_k(\mathbf{x})E_k(\mathbf{x})\rangle + \langle H_k(\mathbf{x})H_k(\mathbf{x})\rangle\right]\right\}, \qquad 20.$$

where the correlators are evaluated for equal times $t = t'$. To gain further insight, we note that at points $\mathbf{x}$ and $\mathbf{x}'$, both lying in the vacuum medium, the Green's functions $\mathcal{G}_{ij}^{(\alpha\beta)}(\mathbf{x}, \mathbf{x}'; \omega)$ can be decomposed as follows:

$$\mathcal{G}_{ij}^{(\alpha\beta)}(\mathbf{x}, \mathbf{x}'; \omega) = \mathcal{G}_{ij}^{(\alpha\beta;0)}(\mathbf{x} - \mathbf{x}'; \omega) + \Gamma_{ij}^{(\alpha\beta)}(\mathbf{x}, \mathbf{x}'; \omega), \quad 21.$$

where $\mathcal{G}_{ij}^{(\alpha\beta;0)}(\mathbf{x} - \mathbf{x}'; \omega)$ is the Green's function of free space and $\Gamma_{ij}^{(\alpha\beta)}(\mathbf{x}, \mathbf{x}'; \omega)$ describes the EM field scattered by the bodies. When the above decomposition is used in Equation 20, the expectation value of the stress tensor is decomposed accordingly as

$$\langle T_{ij}(\mathbf{x}) \rangle = \langle T_{ij}^{(0)}(\mathbf{x}) \rangle + \Theta_{ij}(\mathbf{x}), \quad 22.$$

where $\langle T_{ij}^{(0)}(\mathbf{x}) \rangle$ is the free-space contribution and $\Theta_{ij}(\mathbf{x})$ is the scattering contribution. According to Equation 19, $\langle T_{ij}^{(0)}(\mathbf{x}) \rangle$ and $\Theta_{ij}(\mathbf{x})$ involve frequency integrals of the imaginary parts of the respective Green's functions $\mathcal{G}_{ij}^{(\alpha\beta;0)}(\mathbf{x}, \mathbf{x}'; \omega)$ and $\Gamma_{ij}^{(\alpha\beta)}(\mathbf{x}, \mathbf{x}'; \omega)$.

Let us consider $\langle T_{ij}^{(0)}(\mathbf{x}) \rangle$ first. Because

$$\lim_{\mathbf{x}\to\mathbf{x}'} \mathrm{Im}[\mathcal{G}_{ij}^{(EE;0)}(\mathbf{x}, \mathbf{x}', \omega)] = \lim_{\mathbf{x}\to\mathbf{x}'} \mathrm{Im}[\mathcal{G}_{ij}^{(HH;0)}(\mathbf{x}, \mathbf{x}', \omega)] = \frac{2\,\omega^3}{3\,c^3}\delta_{ij}, \quad 23.$$

it is clear that $\langle T_{ij}^{(0)}(\mathbf{x}) \rangle$ is expressed by a formally divergent frequency integral. Note, however, that according to Equation 23, $\langle T_{ij}^{(0)}(\mathbf{x}) \rangle$ represents a homogeneous and isotropic pressure acting the surfaces of the bodies, which is independent of the material properties of the bodies. Because this pressure cannot give rise to an overall force on the body, only a stress, as discussed above, we can neglect it here.

Let us turn to the scattering contribution $\Theta_{ij}(\mathbf{x})$. By performing a Wick rotation to the imaginary frequency axis, we find that $\Theta_{ij}(\mathbf{x})$ has the expression

$$\Theta_{ij}(\mathbf{x}) = \frac{k_\mathrm{B}T}{2\pi} {\sum_{n=0}^{\infty}}' \Big[\Gamma_{ij}^{(EE)}(\mathbf{x}, \mathbf{x}; \mathrm{i}\,\xi_n) + \Gamma_{ij}^{(HH)}(\mathbf{x}, \mathbf{x}; \mathrm{i}\,\xi_n) - \frac{1}{2}\delta_{ij} \left(\Gamma_{kk}^{(EE)}(\mathbf{x}, \mathbf{x}; \mathrm{i}\,\xi_n) + \Gamma_{kk}^{(HH)}(\mathbf{x}, \mathbf{x}; \mathrm{i}\,\xi_n) \right) \Big], \quad 24.$$

where $\xi_n = 2\pi n k_\mathrm{B}T/\hbar$ are the Matsubara imaginary frequencies, and the prime symbol in the summations means that the $n = 0$ term is taken with a weight of one-half. The sum on the right-hand side of the above equation is finite, because the scattering parts of the Green's functions $\Gamma_{ij}^{(\alpha\beta)}(\mathbf{x}, \mathbf{x}'; \omega)$ remain finite in the coincidence limit $\mathbf{x}' \to \mathbf{x}$.

The Casimir force on body r can be now obtained by integrating $\Theta_{ij}(\mathbf{x})$ on any surface S_r drawn in the vacuum that surrounds that body and excludes all other bodies, yielding

$$F_i^{(r)} = \oint_{S_r} d^2\sigma\, \hat{n}_j(\mathbf{x})\, \Theta_{ji}(\mathbf{x}). \quad 25.$$

The surface integral on the right-hand side of this equation can be recast in a remarkably simple form, by taking advantage of the peculiar structure of the scattering Green's functions $\Gamma_{ij}^{(\alpha\beta)}(\mathbf{x}, \mathbf{x}')$ (for brevity, from now on we do not display the dependence of the Green's functions on the Matsubara frequencies ξ_n). This structure becomes manifest once $\Gamma_{ij}^{(\alpha\beta)}(\mathbf{x}, \mathbf{x}')$ is expressed in terms of the so-called T operator (57, 58). Recall that the T operator $T_{kl}^{(\rho\sigma)}(\mathbf{y}, \mathbf{y}')$ is defined to give the currents induced at the point $\mathbf{y}$ in the interior of the bodies by an external EM field at point $\mathbf{y}'$. Using the T operator, we can express the scattering parts of the Green's functions as

$$\Gamma_{ij}^{(\alpha\beta)}(\mathbf{x}, \mathbf{x}') = \sum_{r,r'=1}^{N} \int_{V_r} d^3\mathbf{y} \int_{V_{r'}} d^3\mathbf{y}'\, \mathcal{G}_{ik}^{(\alpha\rho;0)}(\mathbf{x} - \mathbf{y}) T_{kl}^{(\rho\sigma)}(\mathbf{y}, \mathbf{y}') \mathcal{G}_{lj}^{(\sigma\beta;0)}(\mathbf{y}' - \mathbf{x}'). \quad 26.$$

Despite its simple meaning, the T operator is difficult to compute in general, and its expression is known only for bodies with sufficiently symmetric geometries, mostly in cases where the T operator is diagonal. A more powerful representation of the scattering Green's functions can be derived from the equivalence principle of classical EM theory (131). According to this principle, the induced currents existing in the interior of the bodies can be replaced by fictitious surface currents, which produce the same scattered field as the induced currents. By following this equivalence principle, we arrive at an alternative representation of the scattering Green's functions consisting of a double surface integral extended onto the surfaces of the bodies (129, 130):

$$\Gamma_{ij}^{(\alpha\beta)}(\mathbf{x},\mathbf{x}') = -\sum_{r,r'=1}^{N} \int_{V_r} d^3\mathbf{y} \int_{V_{r'}} d^3\mathbf{y}'\, \delta[F_r(\mathbf{y})]\, \delta[F_{r'}(\mathbf{y}')] \times \mathcal{G}_{ik}^{(\alpha\rho;0)}(\mathbf{x}-\mathbf{y}) \left(M^{-1}\right)_{kl}^{(\rho\sigma)}(\mathbf{y},\mathbf{y}') \mathcal{G}_{lj}^{(\sigma\beta;0)}(\mathbf{y}'-\mathbf{x}'), \quad 27.$$

where $\delta(x)$ is the Dirac delta function and $F_r(\mathbf{y}) = 0$ is the equation of the surface Σ_r of the rth body. The surface operator $M_{ij}^{(\alpha\beta)}(\mathbf{y},\mathbf{y}')$, whose inverse appears in the integral on the right-hand side, has a remarkably simple expression (129, 130):

$$M_{ij}^{(\alpha\beta)}(\mathbf{y},\mathbf{y}') = \begin{cases} \Pi_{ik}^{(r)}(\mathbf{y}) \left[\mathcal{G}_{kl}^{(\alpha\beta;r)}(\mathbf{y}-\mathbf{y}') + \mathcal{G}_{kl}^{(\alpha\beta;0)}(\mathbf{y}-\mathbf{y}')\right] \Pi_{lj}^{(r)}(\mathbf{y}') & \text{if } \mathbf{y},\mathbf{y}' \in \Sigma_r, \\ \Pi_{ik}^{(r)}(\mathbf{y})\, \mathcal{G}_{kl}^{(\alpha\beta;0)}(\mathbf{y}-\mathbf{y}')\, \Pi_{lj}^{(s)}(\mathbf{y}') & \text{if } \mathbf{y} \in \Sigma_r, \tilde{\mathbf{y}}' \in \Sigma_s, \\ & r \neq s. \end{cases} \quad 28.$$

Here, $\Pi_{ik}^{(r)}(\mathbf{y})$ is the projector onto the plane tangent at Σ_r at $\mathbf{y}$, and $\mathcal{G}_{ij}^{(\alpha\beta;r)}(\mathbf{y}-\mathbf{y}')$ are the Green's functions for an infinite homogeneous and isotropic magneto-dielectric medium identical to that of body r. Inspection of Equations 26 and 27 reveals that both representations of the scattering Green's functions have a common $\hat{G}^{(0)}\hat{\mathcal{K}}\,\hat{G}^{(0)}$ structure, where the $\hat{\mathcal{K}}$ operator coincides either with Waterman's T operator or with (minus) the inverse of the surface operator $\hat{M}$. Importantly, both the T operator and the surface operator $\hat{M}$ satisfy the reciprocity relations (131) enjoyed by the Green's functions. Reference 130 shows that whenever the scattering Green's function has the $\hat{G}^{(0)}\hat{\mathcal{K}}\,\hat{G}^{(0)}$ structure, with a $\hat{\mathcal{K}}$ satisfying reciprocity, the force formula in Equation 25 can be recast in the remarkably simple form

$$\mathbf{F}^{(r)} = k_B T \sum_{n=0}^{\infty}{}' \mathrm{Tr}\left[\hat{\mathcal{K}}(\mathrm{i}\,\xi_n) \frac{\partial}{\partial \mathbf{x}_r} \hat{\mathcal{G}}^{(0)}(\mathrm{i}\,\xi_n)\right], \quad 29.$$

where the trace operation Tr denotes an integral over the volumes occupied by the bodies and a sum over both the spatial indices i and j and the internal indices α and β, and the symbol $\partial/\partial\mathbf{x}_r$ denotes a derivative with respect to a rigid translation of the rth body. When $\hat{\mathcal{K}}$ is identified with the T operator, Equation 29 reproduces the TGTG formula derived in Reference 59. If $\hat{\mathcal{K}}$ is instead identified with (minus) the surface operator $(\hat{M})^{-1}$, then Equation 29 reproduces the surface force formula derived in Reference 129. Thus, Equation 29 encompasses in a single compact formula the bulk and surface formulations of the Casimir force.

Starting from Equation 29, it is possible to compute the Casimir free energy of the system of bodies. Direct integration of Equation 29 leads to a formally divergent result, $\mathcal{F}_{\mathrm{bare}}$. However, a finite expression is easily recovered by subtracting from $\mathcal{F}_{\mathrm{bare}}$ the self-energies of the individual bodies. The details of the subtraction procedure differ slightly within the bulk and surface formulations, but the final formula for the renormalized Casimir free energy $\mathcal{F}$ has an identical form in

both approaches (130). In the simple case of two bodies, it reads

$$\mathcal{F} = k_B T \sum_{n=0}^{\infty}{}' \mathrm{Tr}\, \log\left[1 - \hat{\mathcal{K}}_1 \hat{\mathcal{G}}^{(0)} \hat{\mathcal{K}}_2 \hat{\mathcal{G}}^{(0)}\right]. \qquad 30.$$

Within the bulk approach, the operator $\hat{\mathcal{K}}_r$ coincides with the T operator $T_{ij}^{(\alpha\beta;r)}(\mathbf{y},\mathbf{y}')$ of body r in isolation, while in the surface approach $\hat{\mathcal{K}}_r$ coincides with (minus) the inverse of the surface operator $M_{ij}^{(\alpha\beta;r)}(\mathbf{y},\mathbf{y}')$, defined by the first line of Equation 28.

We emphasize that Equations 29 and 30 are valid for any shape and relative disposition of the bodies. In particular, both equations hold for a system of interleaved bodies, possibly nested one inside the other. A case deserving special consideration is that of a separable configuration of two bodies, namely a configuration in which the bodies can be separated from each other by a plane drawn in the vacuum between them. Three typical examples of separable configurations are those of a sphere opposite a plate, a system of two spheres, and a sphere and a cylinder, which represent the configurations adopted in the vast majority of experiments. Reference 130 shows that in a separable configuration, the general formula (Equation 30) reproduces the famous scattering formula (22, 63, 85, 90) in which the operators $\hat{\mathcal{K}}_r$ are replaced by the scattering matrices of the bodies and $\hat{\mathcal{G}}^{(0)}$ is replaced by the so-called translation matrices.

4.2. Path Integral Approach

As in Section 4.1, we consider N dielectric bodies with the properties described above. In the Euclidean path integral quantization of the EM field, the Casimir free energy at finite temperature T can be obtained as

$$\mathcal{F} = -k_B T \sum_{n=0}^{\infty}{}' \log \frac{\mathcal{Z}(\xi_n)}{\mathcal{Z}_\infty(\xi_n)}, \qquad 31.$$

where again the sum runs over the Matsubara frequencies $\xi_n = 2\pi n k_B T/\hbar$, with a weight of $1/2$ for $n = 0$. The partition function $\mathcal{Z}$ is given by a path integral that we now derive. The partition function $\mathcal{Z}_\infty$ describes the configuration of infinitely separated bodies and subtracts the self-energies of the bodies from the bare free energy.

We express the action of the EM field in the absence of free sources in terms of the gauge field $\mathbf{A}$. We choose the transverse gauge with $A_0 = 0$. The functional integral then runs over $\mathbf{A}$ only. The electric field is given by $\mathbf{E} = ik\mathbf{A} \to -\kappa\mathbf{A}$, and the magnetic field is given by $\mathbf{B} = \nabla \times \mathbf{A}$. The action in terms of the induced sources at fixed frequency κ is then given by

$$\hat{S}[\mathbf{A}] = -\frac{1}{2}\int_{\mathbb{R}^3} d^3\mathbf{x}\left[\mathbf{A}^2 \epsilon_{\mathbf{x}} \kappa^2 + \frac{1}{\mu_{\mathbf{x}}}(\nabla \times \mathbf{A})^2\right] - \kappa \sum_{r=1}^{N}\int_{V_r} d^3\mathbf{x}\, \mathbf{A}\cdot\mathbf{P}_r \qquad 32.$$

for fluctuations $\mathbf{A}$ of the gauge field and induced bulk currents $\mathbf{P}_r$ inside the objects. The inverse of the kernel of the quadratic part of this action is given by the Green's tensor, which for spatially constant ϵ_r and μ_r of body r is given by

$$\overleftrightarrow{\mathcal{G}}^{(AA;r)}(\mathbf{x},\mathbf{x}') = \mu_r\left(\mathbf{1} - \frac{1}{\epsilon_r \mu_r \kappa^2}\nabla\otimes\nabla\right)\frac{e^{-\sqrt{\epsilon_r\mu_r}\kappa|\mathbf{x}-\mathbf{x}'|}}{|\mathbf{x}-\mathbf{x}'|}. \qquad 33.$$

From the relation between the gauge field $\mathbf{A}$ and the electric field $\mathbf{E}$, the relation $-\kappa^2 \overleftrightarrow{\mathcal{G}}^{(AA;r)}(\mathbf{x},\mathbf{x}') = \overleftrightarrow{\mathcal{G}}^{(EE;r)}(\mathbf{x},\mathbf{x}')$ follows, allowing us to compare the results below with those of the stress tensor–based derivation. Next, we define the classical solutions $\boldsymbol{\mathcal{A}}_r$ of the vector wave

equation in each region V_r, obeying $\nabla \times \nabla \times \boldsymbol{\mathcal{A}}_r + \epsilon_r \mu_r \kappa^2 \boldsymbol{\mathcal{A}}_r = -\kappa \mu_r \mathbf{P}_r$. The source terms of Equation 32 can then be written as an integral over the surface of the body:

$$-\kappa \int_{V_r} d^3\mathbf{x} \mathbf{A} \cdot \mathbf{P}_r = \frac{1}{\mu_r} \int_{\Sigma_r} d^3\mathbf{x} \Big(\mathbf{A}_- \cdot [\mathbf{n}_r \times (\nabla \times \boldsymbol{\mathcal{A}}_r)] + (\nabla \times \mathbf{A})_- \cdot (\mathbf{n}_r \times \boldsymbol{\mathcal{A}}_r) \Big). \quad 34.$$

The values of the gauge field $\mathbf{A}$ and its curl $\nabla \times \mathbf{A}$ appearing in this expression are those obtained when the surface is approached from the inside, denoted by $\mathbf{A}_-$ and $(\nabla \times \mathbf{A})_-$. Note that in the above surface integral, $\mathbf{A}$ and $\nabla \times \mathbf{A}$ multiply vectors that are tangential to the surface; therefore, only the tangential components of $\mathbf{A}$ and $\nabla \times \mathbf{A}$ contribute to the integral. Thus, we can use the continuity conditions of the tangential components of $\mathbf{E}$ and $\mathbf{H}$,

$$\mathbf{n}_r \times \mathbf{E}_- = \mathbf{n}_r \times \mathbf{E}_+, \quad \frac{1}{\mu_r} \mathbf{n}_r \times (\nabla \times \mathbf{E})_- = \frac{1}{\mu_0} \mathbf{n}_r \times (\nabla \times \mathbf{E})_+, \quad 35.$$

to write the source terms also as

$$-\kappa \int_{V_r} d^3\mathbf{x} \mathbf{A} \cdot \mathbf{P}_r = \int_{\Sigma_r} d^3\mathbf{x} \Big(\frac{1}{\mu_r} \mathbf{A}_+ \cdot [\mathbf{n}_r \times (\nabla \times \boldsymbol{\mathcal{A}}_r)] + \frac{1}{\mu_0} (\nabla \times \mathbf{A})_+ \cdot (\mathbf{n}_r \times \boldsymbol{\mathcal{A}}_r) \Big), \quad 36.$$

where the values of the gauge field $\mathbf{A}$ and its curl $\nabla \times \mathbf{A}$ appearing in this expression are now those obtained when the surface is approached from the outside, denoted by $\mathbf{A}_+$ and $(\nabla \times \mathbf{A})_+$.

Now we shall see the advantage of having expressed the source integrals in terms of the values of $\mathbf{A}$ and $\nabla \times \mathbf{A}$ when the surfaces are approached from either the outside or the inside of the objects. In the region V_0, the field $\mathbf{A} \equiv \mathbf{A}_0$ is fully determined by its values on the surfaces Σ_r and by ϵ_0 and μ_0, which are constant across V_0. When integrating out $\mathbf{A}_0$, we compute the two-point correlation function of $\mathbf{A}_+$ and $(\nabla \times \mathbf{A})_+$ on the surfaces Σ_r, so the behavior of $\mathbf{A}_0$ inside the regions V_r with $r > 0$ is irrelevant. Following the same arguments for $\mathbf{A} \equiv \mathbf{A}_r$ inside the objects, we find that the behavior of $\mathbf{A}_r$ outside of region V_r is irrelevant for computing the correlations of $\mathbf{A}_-$ and $(\nabla \times \mathbf{A})_-$ on the surfaces Σ_r. Therefore, we can replace in the action the spatially dependent $\epsilon_\mathbf{x}$ by ϵ_0 when the coupling of $\mathbf{A}_0$ to the surface fields $\boldsymbol{\mathcal{A}}_r$ is represented by Equation 36, and similarly we replace $\epsilon_\mathbf{x}$ by ϵ_r when the coupling of $\mathbf{A}_r$ to the surface fields $\boldsymbol{\mathcal{A}}_r$ is represented by Equation 34.

That this choice is justified can also be understood as follows. The field $\mathbf{A}_0$ in region V_0 can be expanded in a basis of functions that obey the wave equation with ϵ_0. The same can be done for $\mathbf{A}_r$ in the interior of each object; in other words, $\mathbf{A}_r$ can be expanded in a basis of functions that obey the wave equation with ϵ_r in V_r. For each given set of expansion coefficients in V_0 there are corresponding coefficients within each region V_r that are determined by the continuity conditions at the surfaces Σ_r. The functional integral over $\mathbf{A}$ then corresponds to integrating over consistent sets of expansion coefficients that are related by the continuity conditions. The two-point correlations of $\mathbf{A}_+$ and $(\nabla \times \mathbf{A})_+$ on the surfaces Σ_r are then fully determined by the integral over the expansion coefficients of $\mathbf{A}_0$ in V_0 only, and the interior expansion coefficients play no role. Equivalently, the two-point correlations of $\mathbf{A}_-$ and $(\nabla \times \mathbf{A})_-$ on the surfaces Σ_r are then fully determined by the integral over the expansion coefficients of $\mathbf{A}_r$ in V_r only, and now the exterior expansion coefficients are irrelevant. Thus, in the functional integral, the integration of $\mathbf{A}$ can be replaced by $N + 1$ integrations over the fields $\mathbf{A}_r$ and $r = 0, \ldots, N$, where each $\mathbf{A}_r$ is allowed to extend over unbounded space with the action for a free field in a homogeneous space with ϵ_r and μ_r. The multiple counting of degrees of freedom that results from $N + 1$ functional integrations poses no problem, because the (formally infinite) factor in the partition function cancels when the Casimir energy is computed from Equation 31.

With this representation, we can write the partition function as a functional integral over the fluctuations $\mathbf{A}_r$, separately in each region V_r, and the surface fields $\boldsymbol{\mathcal{A}}_r$ on body r, with the action

$$\begin{aligned}\hat{S}[\{\mathbf{A}_r\},\{\boldsymbol{\mathcal{A}}_r\}] = &-\frac{1}{2}\sum_{r=0}^{N}\int_{\mathbb{R}^3} d^3\mathbf{x}\left[\mathbf{A}_r^2\epsilon_r\kappa^2 + \frac{1}{\mu_r}(\nabla\times\mathbf{A}_r)^2\right]\\ &+\sum_{r=1}^{N}\int_{\Sigma_r} d^3\mathbf{x}\left[\frac{1}{\mu_r}\mathbf{A}_0[\mathbf{n}_r\times(\nabla\times\boldsymbol{\mathcal{A}}_r)] + \frac{1}{\mu_0}(\nabla\times\mathbf{A}_0)(\mathbf{n}_r\times\boldsymbol{\mathcal{A}}_r)\right]\\ &+\sum_{r=1}^{N}\int_{\Sigma_r} d^3\mathbf{x}\left[\frac{1}{\mu_r}\mathbf{A}_r[\mathbf{n}_r\times(\nabla\times\boldsymbol{\mathcal{A}}_r)] + \frac{1}{\mu_r}(\nabla\times\mathbf{A}_r)(\mathbf{n}_r\times\boldsymbol{\mathcal{A}}_r)\right]. \qquad 37.\end{aligned}$$

Now we can easily integrate out the fluctuations $\mathbf{A}_r$, noting that the two-point correlation function $\langle\mathbf{A}_r(\mathbf{x})\mathbf{A}_{r'}(\mathbf{x}')\rangle$ equals zero for all $r, r' = 0,\ldots,N$, where $r\neq r'$. This yields the partition function

$$\begin{aligned}\mathcal{Z}(\xi) = \prod_{r=1}^{N}\int\mathcal{D}\boldsymbol{\mathcal{A}}_r \exp\Bigg[-\frac{\beta}{2}\Bigg(&\sum_{r=1}^{N}\int_{\Sigma_r} d^3\mathbf{x}\int_{\Sigma_r} d^3\mathbf{x}'\,\boldsymbol{\mathcal{A}}_r(\mathbf{x})L_r(\mathbf{x},\mathbf{x}')\boldsymbol{\mathcal{A}}_r(\mathbf{x}')\\ &+\sum_{r,r'=1}^{N}\int_{\Sigma_r} d^3\mathbf{x}\int_{\Sigma_{r'}} d^3\mathbf{x}'\,\boldsymbol{\mathcal{A}}_r(\mathbf{x})M_{rr'}(\mathbf{x},\mathbf{x}')\boldsymbol{\mathcal{A}}_{r'}(\mathbf{x}')\Bigg)\Bigg] \qquad 38.\end{aligned}$$

with the kernels

$$\begin{aligned}L_r(\mathbf{x},\mathbf{x}') = \frac{1}{\mu_r^2}\Big[&\nabla\times\nabla\times\overleftrightarrow{\mathcal{G}}^{(AA;r)}(\mathbf{x},\mathbf{x}')(\mathbf{n}_r\times\overleftarrow{\cdot})(\mathbf{n}_r'\times\overrightarrow{\cdot})\\ &+\nabla\times\overleftrightarrow{\mathcal{G}}^{(AA;r)}(\mathbf{x},\mathbf{x}')[\mathbf{n}_r\times(\nabla\times\overleftarrow{\cdot})](\mathbf{n}_r'\times\overrightarrow{\cdot})\\ &+\nabla\times\overleftrightarrow{\mathcal{G}}^{(AA;r)}(\mathbf{x},\mathbf{x}')(\mathbf{n}_r\times\overleftarrow{\cdot})[\mathbf{n}_r'\times(\nabla'\times\overrightarrow{\cdot})]\\ &+\overleftrightarrow{\mathcal{G}}^{(AA;r)}(\mathbf{x},\mathbf{x}')[\mathbf{n}_r\times(\nabla\times\overleftarrow{\cdot})][\mathbf{n}_r'\times(\nabla'\times\overrightarrow{\cdot})]\Big],\\ M_{rr'}(\mathbf{x},\mathbf{x}') = \frac{1}{\mu_0^2}&\nabla\times\nabla\times\overleftrightarrow{\mathcal{G}}^{(AA;0)}(\mathbf{x},\mathbf{x}')(\mathbf{n}_r\times\overleftarrow{\cdot})(\mathbf{n}_{r'}'\times\overrightarrow{\cdot})\\ &+\frac{1}{\mu_0\mu_r}\nabla\times\overleftrightarrow{\mathcal{G}}^{(AA;0)}(\mathbf{x},\mathbf{x}')[\mathbf{n}_r\times(\nabla\times\overleftarrow{\cdot})](\mathbf{n}_{r'}'\times\overrightarrow{\cdot})\\ &+\frac{1}{\mu_0\mu_{r'}}\nabla\times\overleftrightarrow{\mathcal{G}}^{(AA;0)}(\mathbf{x},\mathbf{x}')(\mathbf{n}_r\times\overleftarrow{\cdot})[\mathbf{n}_{r'}'\times(\nabla'\times\overrightarrow{\cdot})]\\ &+\frac{1}{\mu_r\mu_{r'}}\overleftrightarrow{\mathcal{G}}^{(AA;0)}(\mathbf{x},\mathbf{x}')[\mathbf{n}_r\times(\nabla\times\overleftarrow{\cdot})][\mathbf{n}_{r'}'\times(\nabla'\times\overrightarrow{\cdot})], \qquad 39.\end{aligned}$$

where the arrow over the placeholder $\cdot$ indicates to which side of the kernel it acts. This notation implies that the derivatives are taken before the kernel is evaluated with $\mathbf{x}$ and $\mathbf{x}'$ on the surfaces Σ_r; in other words, information about the behavior of basis functions is required in an infinitesimal vicinity of the surfaces. There is an important simplification of this representation: The bilinear form described by the kernel L_r is degenerate on the space of functions over which the functional

integral runs; that is, $\int_{\Sigma_r} d^3\mathbf{x} \int_{\Sigma_r} d^3\mathbf{x}' \boldsymbol{\mathcal{A}}_r(\mathbf{x}) L_r(\mathbf{x},\mathbf{x}') \boldsymbol{\mathcal{A}}_r(\mathbf{x}') = 0$ for all $\boldsymbol{\mathcal{A}}_r(\mathbf{x})$ that are regular solutions of the vector wave equation $\nabla \times \nabla \times \boldsymbol{\mathcal{A}}_r + \epsilon_r \mu_r \kappa^2 \boldsymbol{\mathcal{A}}_r = 0$ inside region V_r. This implies that the kernel L_r can be ignored in the above functional integral over regular waves $\boldsymbol{\mathcal{A}}_r$ inside the objects, and the partition function in Equation 31 is given by the functional determinant of the kernel $M_{rr'}$ alone, which can be computed in some basis for regular waves inside the bodies, evaluated at the surfaces only.

The representation of the partition function thus obtained sums over all configurations of the surface fields $\boldsymbol{\mathcal{A}}_r$, and the action depends on both $\boldsymbol{\mathcal{A}}_r$ and the tangential part of its curl, which is functionally dependent on $\boldsymbol{\mathcal{A}}_r$. Therefore, the situation is similar to classical mechanics, where the Lagrangian depends on the trajectory $q(t)$ and its velocity $\dot{q}(t)$. The Lagrangian path integral then runs over all of path $q(t)$, with $\dot{q}(t)$ determined by the path automatically. To obtain a representation in terms of a space of functions that are defined strictly on the surfaces Σ_r only, it would be useful to be able to integrate over $\boldsymbol{\mathcal{A}}_r$ and its derivatives independently. In classical mechanics, one does so by using Lagrange multipliers that lead to a Legendre transformation of the action to its Hamiltonian form. Here the situation is similar. Let us consider the part of the action, S_r, which, after functional integration over $\mathbf{A}_r$, generates the kernel L_r, which above was shown to vanish. The exponential of this part of the action can be written as a functional integral over two new vector fields $\mathbf{K}_r$ and $\mathbf{K}'_r$ that are defined on the surfaces Σ_r and are tangential to the surfaces,

$$
\begin{aligned}
&\exp(-\beta S_r) \\
&= \mathcal{Z}_r \oint \mathcal{D}\mathbf{K}_r \mathcal{D}\mathbf{K}'_r \exp\left\{ -\frac{\beta}{2} \frac{1}{\mu_r^2} \int_{\Sigma_r} d^3\mathbf{x} \int_{\Sigma_r} d^3\mathbf{x}' \left[\mathbf{K}_r(\mathbf{x}) \cdot \nabla \times \nabla \times \overleftrightarrow{\mathcal{G}}^{(AA;r)}(\mathbf{x},\mathbf{x}') \cdot \mathbf{K}_r(\mathbf{x}') \right.\right. \\
&\quad + \mathbf{K}_r(\mathbf{x}) \cdot \nabla \times \overleftrightarrow{\mathcal{G}}^{(AA;r)}(\mathbf{x},\mathbf{x}') \cdot \mathbf{K}'_r(\mathbf{x}') + \mathbf{K}'_r(\mathbf{x}) \cdot \nabla \times \overleftrightarrow{\mathcal{G}}^{(AA;r)}(\mathbf{x},\mathbf{x}') \cdot \mathbf{K}_r(\mathbf{x}') \\
&\quad \left.\left. + \mathbf{K}'_r(\mathbf{x}) \cdot \overleftrightarrow{\mathcal{G}}^{(AA;r)}(\mathbf{x},\mathbf{x}') \cdot \mathbf{K}'_r(\mathbf{x}') \right] \right. \\
&\quad \left. + \frac{1}{\mu_r} \int_{\Sigma_r} d^3\mathbf{x} \left(\mathbf{A}_r \cdot [\mathbf{n}_r \times (\nabla \times \boldsymbol{\mathcal{A}}_r) - \mathbf{K}'_r] + (\nabla \times \mathbf{A}_r) \cdot (\mathbf{n}_r \times \boldsymbol{\mathcal{A}}_r - \mathbf{K}_r) \right) \right\}, \qquad 40.
\end{aligned}
$$

where $\mathcal{Z}_r$ is some normalization coefficient, and we have used $\oint \mathcal{D}\mathbf{K}_r \mathcal{D}\mathbf{K}'_r$ to indicate that the functional integral extends only over vector fields that are tangential to the surface Σ_r. This representation shows that the $\mathbf{A}_r$ acts as a Lagrange multiplier. Integration over this field removes the imposed constraints between the dependent tangential fields $\mathbf{n}_r \times \boldsymbol{\mathcal{A}}_r$ and $\mathbf{n}_r \times (\nabla \times \boldsymbol{\mathcal{A}}_r)$ by replacing them with the independent tangential surface currents $\mathbf{K}_r$ and $\mathbf{K}'_r$, respectively.

Substituting Equation 40 for each object into the expression for the partition function, integrating out the fields $\mathbf{A}_r$ for $r = 1, \ldots, N$, constraining the functional integral over $\boldsymbol{\mathcal{A}}_r$ to be replaced by the substitutions $\mathbf{n}_r \times \boldsymbol{\mathcal{A}}_r \to \mathbf{K}_r$ and $\mathbf{n}_r \times (\nabla \times \boldsymbol{\mathcal{A}}_r) \to \mathbf{K}'_r$, and finally integrating out $\mathbf{A}_0$, we find

$$
\begin{aligned}
\mathcal{Z}(\xi) = \prod_{r=1}^{N} \oint \mathcal{D}\underline{\mathbf{K}}_r \exp\left[-\frac{\beta}{2} \left(\sum_{r=1}^{N} \int_{\Sigma_r} d^3\mathbf{x} \int_{\Sigma_r} d^3\mathbf{x}' \, \underline{\mathbf{K}}_r(\mathbf{x}) \hat{L}_r(\mathbf{x},\mathbf{x}') \underline{\mathbf{K}}_r(\mathbf{x}') \right.\right. \\
\left.\left. + \sum_{r,r'=1}^{N} \int_{\Sigma_r} d^3\mathbf{x} \int_{\Sigma_{r'}} d^3\mathbf{x}' \, \underline{\mathbf{K}}_r(\mathbf{x}) \hat{M}_{rr'}(\mathbf{x},\mathbf{x}') \underline{\mathbf{K}}_{r'}(\mathbf{x}') \right) \right], \qquad 41.
\end{aligned}
$$

with the kernels

$$\hat{L}_r(\mathbf{x},\mathbf{x}') = \frac{1}{\mu_r^2}\begin{pmatrix} \nabla\times\nabla\times\overleftrightarrow{\mathcal{G}}^{(AA;r)}(\mathbf{x},\mathbf{x}') & \nabla\times\overleftrightarrow{\mathcal{G}}^{(AA;r)}(\mathbf{x},\mathbf{x}') \\ \nabla\times\overleftrightarrow{\mathcal{G}}^{(AA;r)}(\mathbf{x},\mathbf{x}') & \overleftrightarrow{\mathcal{G}}^{(AA;r)}(\mathbf{x},\mathbf{x}') \end{pmatrix}, \tag{42.}$$

$$\hat{M}_{rr'}(\mathbf{x},\mathbf{x}') = \begin{pmatrix} \frac{1}{\mu_0^2}\nabla\times\nabla\times\overleftrightarrow{\mathcal{G}}^{(AA;0)}(\mathbf{x},\mathbf{x}') & \frac{1}{\mu_0\mu_{r'}}\nabla\times\overleftrightarrow{\mathcal{G}}^{(AA;0)}(\mathbf{x},\mathbf{x}') \\ \frac{1}{\mu_0\mu_r}\nabla\times\overleftrightarrow{\mathcal{G}}^{(AA;0)}(\mathbf{x},\mathbf{x}') & \frac{1}{\mu_r\mu_{r'}}\overleftrightarrow{\mathcal{G}}^{(AA;0)}(\mathbf{x},\mathbf{x}') \end{pmatrix}. \tag{43.}$$

We note again that the functional integral in Equation 41 runs over tangential vector fields $\mathbf{K}_r$ and $\mathbf{K}'_r$ defined on the surfaces Σ_r only. The kernels $\hat{L}$ and $\hat{M}$ can be combined into the joint kernel $\hat{N}_{rr'} = \hat{L}_r\delta_{rr'} + \hat{M}_{rr'}$. With this kernel, the Casimir free energy is given by

$$\mathcal{F} = -k_\mathrm{B}T\sum_{n=0}^{\infty}{}' \log\det\left[\hat{N}(\kappa_n)\hat{N}_\infty^{-1}(\kappa_n)\right], \tag{44.}$$

where the determinant runs over all indices; that is, $\mathbf{x}$ and $\mathbf{x}'$ are located on the surfaces Σ_r, and $r, r' = 1,\ldots,N$. The kernel $\hat{N}_\infty$ is obtained from the kernel $\hat{N}$ by taking the distance between all bodies to infinity, that is, by setting $\hat{M}_{rr'} = 0$ for all $r \neq r'$.

The stress tensor approach and the Hamiltonian version of the path integral representation are equivalent to the one derived by Johnson and colleagues (129) as a purely numerical approach using Lagrange multipliers to enforce the boundary conditions in the path integral. Interestingly, the derivation of this representation, presented here from a Lagrangian path integral, demonstrates the relation of this approach to the scattering approach when the T matrix is defined, as originally done by Waterman (57), by surface integrals of regular solutions of the wave equation over the bodies' surfaces. This result shows the close connection of these approaches, motivating further research in the direction of new semianalytical methods to compute Casimir forces.

5. DISCUSSION AND OPEN PROBLEMS

Although the Casimir energy is usually described as a force arising from fluctuations in empty space, as we have shown, it can also be profitably reexpressed in terms of surface currents. A particularly striking open problem for which surface approaches may offer new insights is the contribution of zero-frequency modes to Casimir forces arising from thermal fluctuations.

As indicated in the preceding section, at nonzero temperature T one simply replaces the continuous integral over wave number κ by a sum over Matsubara modes:

$$\int_0^\infty d\kappa \Rightarrow \frac{2\pi k_\mathrm{B}T}{\hbar c}\sum_{n=0}^{\infty}{}', \quad \text{with} \quad \kappa \Rightarrow \kappa_n = \frac{2\pi n k_\mathrm{B}T}{\hbar c}. \tag{45.}$$

Here, again, the prime on the sum indicates that the $n = 0$ mode is counted with a weight of 1/2. In the limit of small T, the sum is well approximated by the zero-temperature integral, while for large T, it is dominated by the $n = 0$ term. In this form, the sum captures the combined effects of thermal and quantum fluctuations.

Because for practical reasons most Casimir experiments are carried out at room temperature, thermal effects can play an important role (133–137). Distance scales at which both the separation between objects can be consistently maintained and the materials act as strong reflectors of light typically correspond to optical frequencies, which then provide the dominant quantum fluctuations. Thermal effects, however, introduce an additional length scale, which at room temperature

is an order of magnitude larger. One would expect to describe fluctuations in a metal by using the Drude model for its permittivity (138, 139):

$$\epsilon(\omega, T) = 1 - \frac{\omega_{\rm p}^2}{\omega[\omega + i\gamma(T)]}. \qquad 46.$$

Here, $\omega_{\rm p}$ is the plasma frequency and $\gamma(T)$ is the relaxation frequency. This model describes an ordinary conductor, which reflects at all nonzero frequencies but can be penetrated by a static magnetic field. In the limit where $\gamma \to 0$, the material becomes nondissipative, described instead by the plasma model. In this limit, we have a superconductor (140, 141), which expels all magnetic fields. The key difference in the Casimir force these models predict thus arises from the contribution of the zero-frequency transverse electric (TE) mode, which now gives a discrete contribution to the Matsubara sum rather than an infinitesimal contribution to a continuous integral at zero temperature. In the Drude model this mode is not scattered appreciably by the metal, whereas in the plasma model it is perfectly reflected.

As a result, for the plasma model, one obtains the interaction free energy per unit area between parallel plates in the perfect conductor limit, for $a \ll \lambda_T$:

$$\frac{\mathcal{F}}{\hbar c A} = -\frac{\pi^2}{720a^3} - \frac{\zeta(3)}{2\pi}\left(\frac{k_{\rm B}T}{\hbar c}\right)^3 + \frac{\pi^2 a}{45}\left(\frac{k_{\rm B}T}{\hbar c}\right)^4 \qquad \text{(plasma model).} \qquad 47.$$

By contrast, for the Drude model calculation, one must subtract

$$\frac{\mathcal{F}_0}{A} = \frac{k_{\rm B}T}{4\pi}\int_0^\infty k_\perp \log\left(1 - e^{-2k_\perp a}\right) dk_\perp = -\frac{\zeta(3)}{16\pi a^2} k_{\rm B}T \qquad 48.$$

to account for the missing TE zero-mode contribution.

Of course, quantum fluctuations of a Drude material do not dissipate energy. Rather, the dissipation arising from the relaxation term represents a coupling between the EM field and the material lattice at equilibrium, which is described by the imaginary-time/temperature-ordered Green's function. Given by $\epsilon^{\rm T}(ic\kappa_n)$, it captures the coupled fluctuations of the EM field and the material degrees of freedom and is symmetric under time reversal, with no dissipation. Experimental scattering data, in contrast, yield the retarded response function $\epsilon^{\rm R}(\omega)$, which is asymmetric in time and does contains dissipation. However, as shown in Reference 22, one can take advantage of the relationship $\epsilon^{\rm T}(ic\kappa_n) = \epsilon^{\rm R}(ic|\kappa_n|)$ (as established in References 142, p. 253, and 143, p. 328) to use the analytic continuation of information obtained about $\epsilon^{\rm R}(ic|\kappa_n|)$, which is accessible to experiment, to calculate $\epsilon^{\rm T}(ic\kappa_n)$, which determines the fluctuation force.

While one would expect the Drude model to provide a more accurate description of real materials with dissipation, both experimental and theoretical considerations argue in favor of the plasma model (144, 145). Most importantly, experiments (146–150) on the whole seem to better match results obtained with the plasma model rather than the Drude model, although the difficult task of achieving the necessary experimental precision is still in progress. At least in the absence of impurities, a purely classical contribution to the free energy like Equation 48 leads to conflict with the Nernst theorem for the entropy at zero temperature. A promising possible solution to this problem involves using a surface impedance model rather than Fresnel scattering, as shown in Reference 151, because the key ambiguity in this mystery seems to lie in the behavior of the surface currents associated with the zero mode. More generally, because zero modes do not represent periodic fluctuations, their quantization frequently introduces subtleties. In soliton physics, for example, collective quantization of zero modes restores translational and rotational symmetry, a process that also requires careful attention to dissipative terms (152).

DISCLOSURE STATEMENT

The authors are not aware of any affiliations, memberships, funding, or financial holdings that might be perceived as affecting the objectivity of this review.

ACKNOWLEDGMENTS

It is a pleasure to thank D. Gelbwaser, R.L. Jaffe, and M. Krüger for conversations and collaboration. N.G. is supported in part by the National Science Foundation (NSF) through grant PHY-1820700. M.K. is supported in part by NSF grant DMR-1708280.

LITERATURE CITED

1. Casimir HBG. *Proc. K. Ned. Akad. Wet.* 51:793 (1948)
2. Lamoreaux SK. *Phys. Rev. Lett.* 78:5 (1997)
3. Mohideen U, Roy A. *Phys. Rev. Lett.* 81:4549 (1998)
4. Roy A, Lin CY, Mohideen U. *Phys. Rev. D* 60:111101 (1999)
5. Ederth T. *Phys. Rev. A* 62:062104 (2000)
6. Chan HB, et al. *Science* 291:1941 (2001)
7. Chen F, Mohideen U, Klimchitskaya GL, Mostepanenko VM. *Phys. Rev. Lett.* 88:101801 (2002)
8. Bressi B, Carugno G, Onofrio R, Ruoso G. *Phys. Rev. Lett.* 88:041804 (2002)
9. Druzhinina V, DeKieviet M. *Phys. Rev. Lett.* 91:193202 (2003)
10. Harber DM, Obrecht JM, McGuirk JM, Cornell EA. *Phys. Rev. A* 72:033610 (2005)
11. Chen F, Klimchitskaya GL, Mostepanenko VM, Mohideen U. *Phys. Rev. Lett.* 97:170402 (2006)
12. Krause DE, Decca RS, López D, Fischbach E. *Phys. Rev. Lett.* 98:050403 (2007)
13. Decca RS, et al. *Phys. Rev. D* 75:077101 (2007)
14. Chen F, Klimchitskaya GL, Mostepanenko VM, Mohideen U. *Phys. Rev. B* 76:035338 (2007)
15. Munday JN, Capasso F. *Phys. Rev. A* 75:060102(R) (2007)
16. Chan HB, et al. *Phys. Rev. Lett.* 101:030401 (2008)
17. Kim WJ, et al. *Phys. Rev. A* 78:020101(R) (2008)
18. Palasantzas G, van Zwol PJ, De Hosson JTM. *Appl. Phys. Lett.* 93:121912 (2008)
19. Munday JN, Capasso F, Parsegian VA. *Nature* 457:170 (2009)
20. Bimonte G, López D, Decca RS. *Phys. Rev. B* 93:184434 (2016)
21. Capasso F, Munday JN, Iannuzzi D, Chan HB. *IEEE J. Sel. Top. Quant.* 13:400 (2007)
22. Rahi SJ, et al. *Phys. Rev. D* 80:085021 (2009)
23. Jaffe RL. *Phys. Rev. D* 72:021301 (2005)
24. Milton KA, Shajesh KV, Fulling SA, Parashar P. *Phys. Rev. D* 89:064027 (2014)
25. Riess AG, et al. *Astron. J.* 116:1009 (1998)
26. Perlmutter S, et al. *Astrophys. J.* 517:565 (1999)
27. Weinberg S. *Phys. Rev. Lett.* 59:2607 (1987)
28. Tsujikawa S. *Class. Quantum Gravity* 30:214003 (2013)
29. Leonhardt U. *Ann. Phys.* 411:167973 (2019)
30. Derjaguin B. *Phys. Rev. D* 69:1435 (1934)
31. Parsegian VA. *Van der Waals Forces: A Handbook for Biologists, Chemists, Engineers, and Physicists*. Cambridge, UK: Cambridge Univ. Press (2005)
32. Lifshitz EM. *Sov. Phys. JETP* 2:73 (1956)
33. Fosco CD, Lombardo FC, Mazzitelli FD. *Phys. Rev. D* 84:105031 (2011)
34. Emig T, Hanke A, Golestanian R, Kardar M. *Phys. Rev. Lett.* 87:260402 (2001)
35. Neto PAM, Lambrecht A, Reynaud S. *Phys. Rev. A* 72:012115 (2005)
36. Bimonte G, Emig T, Jaffe RL, Kardar M. *Europhys. Lett.* 97:50001 (2012)
37. Bimonte G, Emig T, Kardar M. *Appl. Phys. Lett.* 100:074110 (2012)
38. Krüger M, Golyk VA, Bimonte G, Kardar M. *Europhys. Lett.* 104:41001 (2013)
39. Teo LP. *Phys. Rev. D* 88:045019 (2013)

40. Banishev AA, et al. *Phys. Rev. Lett.* 110:250403 (2013)
41. Voronovich A. *Waves Random Media* 4:337 (1994)
42. Teo LP, Bordag M, Nikolaev V. *Phys. Rev. D* 84:125037 (2011)
43. Bimonte G, et al. *Universe* 7:93 (2021)
44. Bimonte G. *Phys. Rev. D* 98:105004 (2018)
45. Polder D, Van Hove M. *Phys. Rev. B* 4:3303 (1971)
46. Golyk VA, Krüger M, McCauley AP, Kardar M. *Europhys. Lett.* 101:034002 (2013)
47. Pendry JB. *J. Phys. Condens. Matter* 11:6621 (1999)
48. Majumdar A. *Annu. Rev. Mater. Sci.* 29:505 (1999)
49. Shen S, Narayanaswamy A, Chen G. *Nano Lett.* 9:2909 (2009)
50. Rousseau E, et al. *Nat. Photonics* 3:514 (2009)
51. Krüger M, Emig T, Kardar M. *Phys. Rev. Lett.* 106:210404 (2011)
52. Sasihithlu K, Narayanaswamy A. *Phys. Rev. B* 83:161406 (2011)
53. Otey C, Fan S. *Phys. Rev. B* 84:245431 (2011)
54. Casimir HBG, Polder D. *Phys. Rev.* 73:360 (1948)
55. Bimonte G, Emig T, Kardar M. *Phys. Rev. D* 90:081702 (2014)
56. Bimonte G, Emig T, Jaffe RL, Kardar M. *Phys. Rev. A* 94:022509 (2016)
57. Waterman PC. *Proc. IEEE* 53:805 (1965)
58. Waterman PC. *Phys. Rev. D* 3:825 (1971)
59. Kenneth O, Klich I. *Phys. Rev. Lett.* 97:160401 (2006)
60. Kats EI. *Sov. Phys. JETP* 46:109 (1977)
61. Jaekel MT, Reynaud S. *J. Phys. I* 1:1395 (1991)
62. Genet C, Lambrecht A, Reynaud S. *Phys. Rev. A* 67:043811 (2003)
63. Lambrecht A, Maia Neto PA, Reynaud S. *New J. Phys.* 8:243 (2006)
64. Balian R, Duplantier B. *Ann. Phys. N. Y.* 104:300 (1977)
65. Balian R, Duplantier B. *Ann. Phys. N. Y.* 112:165 (1978)
66. Krein MG. *Mat. Sborn.* 33:597 (1953)
67. Krein MG. *Sov. Math. Dokl.* 3:707 (1962)
68. Birman MS, Krein MG. *Sov. Math. Dokl.* 3:740 (1962)
69. Henseler M, Wirzba A, Guhr T. *Ann. Phys. N. Y.* 258:286 (1997)
70. Wirzba A. *Phys. Rep.* 309:1 (1999)
71. Bulgac A, Wirzba A. *Phys. Rev. Lett.* 87:120404 (2001)
72. Bulgac A, Magierski P, Wirzba A. *Phys. Rev. D* 73:025007 (2006)
73. Wirzba A. *J. Phys. A* 41:164003 (2008)
74. Graham N, Quandt M, Weigel H. *Spectral Methods in Quantum Field Theory*. Berlin: Springer (2009)
75. Bordag M, Robaschik D, Wieczorek E. *Ann. Phys. N. Y.* 165:192 (1985)
76. Robaschik D, Scharnhorst K, Wieczorek E. *Ann. Phys. N. Y.* 174:401 (1987)
77. Li H, Kardar M. *Phys. Rev. Lett.* 67:3275 (1991)
78. Li H, Kardar M. *Phys. Rev. A* 46:6490 (1992)
79. Golestanian R, Kardar M. *Phys. Rev. Lett.* 78:3421 (1997)
80. Golestanian R, Kardar M. *Phys. Rev. A* 58:1713 (1998)
81. Emig T, Hanke A, Golestanian R, Kardar M. *Phys. Rev. A* 67:022114 (2003)
82. Büscher R, Emig T. *Phys. Rev. Lett.* 94:133901 (2005)
83. Langbein D. *Theory of van der Waals Attraction*. Berlin/Heidelberg: Springer (1974)
84. Emig T, Jaffe RL, Kardar M, Scardicchio A. *Phys. Rev. Lett.* 96:080403 (2006)
85. Emig T, Graham N, Jaffe R, Kardar M. *Phys. Rev. Lett.* 99:170403 (2007)
86. Emig T. *J. Stat. Mech.* 0804:P04007 (2008)
87. Emig T, Graham N, Jaffe R, Kardar M. *Phys. Rev. D* 77:025005 (2008)
88. Maghrebi MF. *Phys. Rev. D* 83:045004 (2011)
89. Rahi SJ, Kardar M, Emig T. *Phys. Rev. Lett.* 105:070404 (2010)
90. Kenneth O, Klich I. *Phys. Rev. B* 78:014103 (2008)
91. Rahi SJ, Emig T, Jaffe RL, Kardar M. *Phys. Rev. A* 78:012104 (2008)

92. Teo LP. *Phys. Rev. D* 87:045021 (2013)
93. Maia Neto PA, Lambrecht A, Reynaud S. *Phys. Rev. A* 78:012115 (2008)
94. Canaguier-Durand A, et al. *Phys. Rev. Lett.* 102:230404 (2009)
95. Graham N. *Phys. Rev. D* 87:105004 (2013)
96. Graham N, et al. *Phys. Rev. D* 81:061701 (2010)
97. Emig T, Graham N, Jaffe RL, Kardar M. *Phys. Rev. A* 79:054901 (2009)
98. Maghrebi MF, et al. *PNAS* 108:6867 (2011)
99. Kabat D, Karabali D, Nair VP. *Phys. Rev. D* 81:125013 (2010)
100. Maghrebi MF, Jaffe RL, Abravanel R. *Phys. Rev. D* 84:061701 (2011)
101. Gies H, Langfeld K, Moyaerts L. *J. High Energy Phys.* 0306:018 (2003)
102. Meixner J. *Z. Naturforsch.* 3:506 (1948)
103. Emig T, Graham N. *Phys. Rev. A* 94:032509 (2016)
104. Graham N, et al. *Phys. Rev. D* 83:125007 (2011)
105. Maghrebi MF, Graham N. *Europhys. Lett.* 95:14001 (2011)
106. Blose EN, Ghimire B, Graham N, Stratton-Smith J. *Phys. Rev. A* 91:012501 (2015)
107. Bateman H. *Trans. Am. Math. Soc.* 33:817 (1931)
108. Casimir HBG. *Physica* XIX:846 (1953)
109. Boyer TH. *Phys. Rev.* 174:1764 (1968)
110. Milton KA, DeRaad LL Jr., Schwinger JS. *Ann. Phys.* 115:388 (1978)
111. Milton KA. *The Casimir Effect: Physical Manifestations of Zero-Point Energy.* Singapore: World Sci. (2001)
112. Abalo EK, Milton KA, Kaplan L. *J. Phys. A* 45:425401 (2012)
113. Kolomeisky EB, Straley JP, Langsjoen LS, Zaidi H. *J. Phys. A* 43:385402 (2010)
114. Cavalcanti RM. *Phys. Rev. D* 69:065015 (2004)
115. Hertzberg MP, Jaffe RL, Kardar M, Scardicchio A. *Phys. Rev. Lett.* 95:250402 (2005)
116. Jaffe RL, Scardicchio A. *Phys. Rev. Lett.* 92:070402 (2004)
117. Graham N, Quandt M, Weigel H. *Phys. Lett. B* 726:846 (2013)
118. Bordag M, Khusnutdinov N. *Phys. Rev. D* 77:085026 (2008)
119. Barton G. *J. Phys. A* 37:1011 (2001)
120. Leonhardt U, Simpson WMR. *Phys. Rev. D* 84:081701 (2011)
121. Deutsch D, Candelas P. *Phys. Rev. D* 20:3063 (1979)
122. Candelas P. *Ann. Phys.* 143:241 (1982)
123. Symanzik K. *Nucl. Phys. B* 190:1 (1981)
124. Graham N, et al. *Phys. Lett. B* 572:196 (2003)
125. Graham N, et al. *Nucl. Phys. B* 645:49 (2002)
126. Graham N, et al. *Nucl. Phys. B* 677:379 (2004)
127. Schaden M, Spruch L. *Phys. Rev. A* 58:935 (1998)
128. Reid MTH, Rodriguez AW, White J, Johnson SG. *Phys. Rev. Lett.* 103:040401 (2009)
129. Reid MTH, White J, Johnson SG. *Phys. Rev. A* 88:022514 (2013)
130. Bimonte G, Emig T. *Universe* 7:225 (2021)
131. Harrington R. *Time-Harmonic Electromagnetic Fields.* New York: Wiley (2001)
132. Agarwal GS. *Phys. Rev. A* 11:230 (1975)
133. Brevik I, Ellingsen SA, Milton KA. *New J. Phys.* 8:236 (2006)
134. Klimchitskaya GL, Mostepanenko VM. *Contemp. Phys.* 47:131 (2006)
135. Canaguier-Durand A, Neto PAM, Lambrecht A, Reynaud S. *Phys. Rev. Lett.* 104:040403 (2010)
136. Bimonte G. *Phys. Rev. Lett.* 112:240401 (2014)
137. Bordag M, Klimchitskaya GL, Mohideen U, Mostepanenko VM. *Advances in the Casimir Effect*. Oxford, UK: Oxford Univ. Press (2009)
138. Boström M, Sernelius BE. *Phys. Rev. Lett.* 84:4757 (2000)
139. Høye JS, Brevik I, Aarseth JB, Milton KA. *Phys. Rev. E* 67:056116 (2003)
140. Bimonte G. *Phys. Rev. A* 78:062101 (2008)
141. Zandi R, Emig T, Mohideen U. *Phys. Rev. B* 81:195423 (2010)
142. Abrikosov AA, Gorkov LP, Dzyaloshinski IE. *Methods of Quantum Field Theory in Statistical Physics.* New York: Dover (1975)

143. Landau LD, Lifshitz EM. *Statistical Physics*, Part 1, Vol. 5: *Course of Theoretical Physics*. Oxford, UK: Pergamon (1980)
144. Bezerra VB, Klimchitskaya GL, Mostepanenko VM. *Phys. Rev. A* 65:052113 (2002)
145. Mostepanenko VM. *Universe* 7:84 (2021)
146. Sushkov AO, Kim WJ, Dalvit DAR, Lamoreaux SK. *Nat. Phys.* 7:230 (2011)
147. Banishev AA, Klimchitskaya GL, Mostepanenko VM, Mohideen U. *Phys. Rev. Lett.* 110:137401 (2013)
148. Yannopapas V, Tzavala M, Tsetseris L. *Phys. Rev. B* 88:155413 (2013)
149. Castillo-Garza R, et al. *Phys. Rev. B* 88:075402 (2013)
150. Behunin RO, et al. *Phys. Rev. A* 90:062115 (2014)
151. Geyer B, Klimchitskaya GL, Mostepanenko VM. *Phys. Rev. A* 67:062102 (2003)
152. Cherman A, Cohen TD, Dulaney TR, Lynch EM. *Phys. Rev. D* 72:094015 (2005)

Annual Review of Nuclear and Particle Science

Volume 72, 2022

Contents

Errata

An online log of corrections to *Annual Review of Nuclear and Particle Science* articles may be found at http://www.annualreviews.org/errata/nucl